

${}^5_{\Lambda\Lambda}\text{H}$ and ${}^5_{\Lambda\Lambda}\text{He}$ hypernuclei reexamined in halo/cluster effective theory

Ghanashyam Meher^{1,*} and Udit Raha^{1,†}

¹*Department of Physics, Indian Institute of Technology Guwahati, 781 039 Assam, India*

The $J = 1/2$ iso-doublet double- Λ -hypernuclei, namely, ${}^5_{\Lambda\Lambda}\text{H}$ and ${}^5_{\Lambda\Lambda}\text{He}$, are examined as the three-body cluster states, $\Lambda\Lambda t$ ($t \equiv {}^3\text{H}$ or triton) and $\Lambda\Lambda h$ ($h \equiv {}^3\text{He}$ or helion), respectively, in a model independent framework utilizing pionless halo effective theory. Both singlet and triplet states of the constituent ΛT ($T \equiv t, h$) subsystem are used in the elastic channel for the study of ${}^4_{\Lambda}\text{H}-\Lambda$ and ${}^4_{\Lambda}\text{He}-\Lambda$ scattering processes. A prototypical leading order investigation using a sharp momentum cutoff regulator (Λ_c) in the coupled integral equations for each type of the ΛT subsystem spin states, yields identical renormalization group limit cycle behavior when the respective three-body contact interactions are taken close to the unitary limit. Furthermore, irrespective of the type of the elastic channel chosen, almost identical cutoff dependence of the three-body binding energy or the double- Λ -separation energy ($B_{\Lambda\Lambda}$) is obtained for the mirror partners, evidently suggesting good isospin symmetry in these three-body systems. Subsequently, upon normalization of our solutions to the integral equation with respect to a single pair of input data from an *ab initio* potential model analysis for each mirror hypernuclei, yields $B_{\Lambda\Lambda}$ which agrees fairly well with various erstwhile regulator independent potential models for our choice of the cutoff, $\Lambda_c \sim 200$ MeV. This is either consistent with pionless effective theory or with its slightly augmented version with a hard scale of $\Lambda_H \gtrsim 2m_\pi$, where low-energy Λ - Λ interactions dominated by $\pi\pi$ or σ -meson exchange. Finally, to demonstrate the predictability of our effective theory, we present preliminary estimates of the S -wave $\Lambda\Lambda T$ three-body scattering lengths and the Λ -separation energies using a range of currently accepted values of the double- Λ scattering length from a variety of existing phenomenological predictions that is constrained by the recent experimental data from relativistic heavy-ion collisions.

I. INTRODUCTION

The various experimental [1–13] and theoretical [14–26] investigations over several decades on the doubly strange ($S = -2$) s -shell light double- Λ -hypernuclear systems, such as, ${}^3_{\Lambda\Lambda}\text{n}$, ${}^4_{\Lambda\Lambda}\text{n}$, ${}^4_{\Lambda\Lambda}\text{H}$, ${}^4_{\Lambda\Lambda}\text{He}$, ${}^5_{\Lambda\Lambda}\text{H}$, ${}^5_{\Lambda\Lambda}\text{He}$ and ${}^6_{\Lambda\Lambda}\text{He}$, have elicited keen interest in the study of exotic hypernuclei in the strangeness nuclear physics community. Such multistrange systems can provide stringent tests for probing the microscopic mechanisms for the flavor SU(3) baryon-baryon interaction in the strangeness $S = -2$ channel. In particular, essential information about the Λ - Λ interaction is expected to be obtained from these studies, which may hold definitive clues to the long-standing quest for the controversial H -dibaryon, an exotic six-quark ($J = 0, I = 0$) deeply bound state, originally predicted by Jaffe in 1977 using the *bag-model* [14]. Different perspectives regarding the existence of the H particle have been obtained in *ab initio* calculations over the years. For example, the *dispersion relations* based analysis [27] on the ${}^{12}\text{C}(K^-, K^+\Lambda\Lambda X)$ reaction data from the KEK-PS Collaboration [4], yielded an estimate of the ${}^1\text{S}_0$ double- Λ scattering length, namely, $a_{\Lambda\Lambda} = -1.2 \pm 0.6$ fm, that was well at odds with a possible $\Lambda\Lambda$ bound state. While lattice QCD simulations [28–32] with significantly larger pion masses yielded extrapolated results suggesting positive indications of a $\Lambda\Lambda$ bound state, albeit a shallow one in the flavor SU(3) limit. However, apparently by going to the physical point, it tends to get pushed to the

double- Λ threshold, eventually dissolving into the continuum once SU(3) breaking effects are considered [33, 34]. In fact, of late the HAL QCD (2 + 1)-flavor coupled-channel lattice simulation [35] closer to the physical point ($m_\pi^{\text{Lat}} \simeq 146$ MeV, $m_K^{\text{Lat}} \simeq 525$ MeV) has yielded a rather small magnitude of the ${}^1\text{S}_0$ double- Λ scattering length, $a_{\Lambda\Lambda} = -0.81 \pm 0.23$ fm, casting a significant doubt on the very existence of the H -particle. This is consistent with the current theoretically accepted (albeit broad) range, namely, -1.92 fm $\lesssim a_{\Lambda\Lambda} \lesssim -0.5$ fm, set by the fairly recent *thermal correlation model* based investigations [36–38] on *Au + Au Relativistic Heavy-Ion Collisions* (RHIC) data from STAR Collaboration [7], which is unlikely to support any $\Lambda\Lambda$ bound state. It is interesting in this regard that the same RHIC data previously analysed by the STAR Collaboration themselves [7] estimated a positive scattering length, $a_{\Lambda\Lambda} = 1.10 \pm 0.37$ fm. Nevertheless, the rather recent Λ - Λ femtoscopic analysis of p - p and p -Pb collision data from the ALICE Collaboration [12, 13] yielded a $\Lambda\Lambda$ virtual bound state of energy ≈ 3.2 MeV, thereby favoring a scattering length consistent with the above range. In short, although these analyses are clearly equivocal in their resolution of the H particle conjecture, they evidently concur on a weakly attractive Λ - Λ interaction with no deeply bound state.

With the discovery of ${}^6_{\Lambda\Lambda}\text{He}$ in the hybrid-emulsion experiment KEK-E373 [1], so-called the “NAGARA” event, along with indications of the conjectured ${}^4_{\Lambda\Lambda}\text{H}$ bound state in the BNL-AGS E906 production experiment [2], arguments on the existence of double- Λ -hypernuclei have gained a firm foothold fostering a prolific area of modern research. A whole gamut of theoretical investigations on the double- Λ -hypernuclei followed since then. As for the

* ghanashyam@iitg.ac.in

† udit.raha@iitg.ac.in

the $J = 1/2$ iso-doublet mirror partners, namely, ${}_{\Lambda\Lambda}^5\text{H}$ and ${}_{\Lambda\Lambda}^5\text{He}$, until rather recently most of these investigations have been focusing on establishing phenomenological potential models. In particular, there exists both *ab initio* and *cluster* model approaches involving three- and four-body Faddeev-Yakubovsky calculations and variational methods [16–23]. In some of these model analyses, the binding energy difference between the two isospin partners has been studied using dynamical effects of mixing between different channels, such as ΣN , $\Sigma\Sigma$, and ΞN . Of these, it is believed that the dominant contribution arises from the $\Lambda\Lambda - \Xi N$ mixing channel. Because of this channel coupling the value of the hypernuclear binding energy (otherwise, commonly referred to in the literature as the *double- Λ -separation energy*) $B_{\Lambda\Lambda}$ of ${}_{\Lambda\Lambda}^5\text{He}$ significantly exceeds that of ${}_{\Lambda\Lambda}^5\text{H}$. However, such model approaches are often nonsystematic with conflicting conclusions based on *ad hoc* assumptions, whereby little perceptions can be gained regarding the underlying binding mechanisms inherent to these systems. It is, thus, timely to supplement the multitude of the existing model results with a general model-independent prediction based on universal arguments in few-body systems.

In a recent pioneering effort, the first microscopic *pionless effective field theory* ($\not\{EFT}$) based many-body analysis using *Stochastic Variational Method* (SVM) has been reported on some of the lightest double- Λ -hypernuclei for $A \leq 6$ [26]. This kind of *ab initio* Hamiltonian constructed $\not\{EFT}$ technique utilizing only elementary baryonic (NN , $N\Lambda$, $\Lambda\Lambda$ two-body and NNN , $N\Lambda N$, $\Lambda\Lambda\Lambda$ three-body) interactions was first applied to calculations of few-nucleon systems for lattice-nuclei [39–41] and later extended to the analysis of s -shell Λ -hypernuclei [42]. Through a *leading order* (LO) assessment of the onset of double- Λ -hypernuclei binding, the work of Ref. [26] quantitatively demonstrates the robust possibility of the iso-doublet partners (${}_{\Lambda\Lambda}^5\text{H}$, ${}_{\Lambda\Lambda}^5\text{He}$), as the lightest particle stable double- Λ -hypernuclei, thereby discounting ${}_{\Lambda\Lambda}^3\text{n}$, ${}_{\Lambda\Lambda}^4\text{n}$ and ${}_{\Lambda\Lambda}^4\text{H}$ as possible bound states. Interestingly, as a parallel qualitative assessment to supplement the aforementioned rigorous numerical analysis, we re-examine the (${}_{\Lambda\Lambda}^5\text{H}$, ${}_{\Lambda\Lambda}^5\text{He}$) iso-doublet pair in view of a plausible cluster or *halo* nuclear nature using universal arguments in physics. Particularly, in the context of standard $\not\{EFT}$ framework we investigate the correlations between their bound state characteristics and the S -wave (${}_{\Lambda}^4\text{H} - \Lambda$, ${}_{\Lambda}^4\text{He} - \Lambda$) scattering processes, respectively, in the kinematical region below the (${}^3\text{H}$, ${}^3\text{He}$) + Λ + Λ breakup thresholds. In this way, through a prototypical model-independent study we assess the role of low-energy Λ - Λ interactions in giving rise to universal correlations between three-body observables of such s -shell double- Λ -hypernuclei and their possible formations thereof.

A low-energy EFT constitutes a systematic model-independent approach with low-energy observables expanded in a perturbative expansion in terms of a small parameter, namely, $\epsilon \sim Q/\Lambda_H \ll 1$, where Q is a generic small momentum and Λ_H is the ultraviolet (UV) cutoff

scale which limits the applicability of the perturbative scheme. The effective degrees of freedom consistent with the low-energy symmetries of the system are then identified in terms of which the Lagrangian of the system is constructed and expanded in increasing order of derivative interaction. The corresponding coefficients (low-energy constants) are fixed from phenomenological data. The heavy degrees of freedom above the hard scale Λ_H are integrated out and their effects are implicitly encoded in these couplings. In the so-called *halo/cluster* EFT formalism, the ${}_{\Lambda\Lambda}^5\text{H}$ and ${}_{\Lambda\Lambda}^5\text{He}$ systems can be regarded as the double- Λ *halo*-nuclear states, namely, $\Lambda\Lambda t$ ($t \equiv {}^3\text{H}$, i.e., the *triton*) and $\Lambda\Lambda h$ ($h \equiv {}^3\text{He}$, i.e., the *helion*), respectively, with $T \equiv t, h$ being the compact core that can be considered elementary at scales chosen well below the breakup of ${}_{\Lambda}^4\text{H}$ and ${}_{\Lambda}^4\text{He}$.

The erstwhile emulsion works [3, 6, 43] have indicated evidences of particle stable states of ${}_{\Lambda}^4\text{H}$ and ${}_{\Lambda}^4\text{He}$ Λ -hypernuclei. The existence of these states were recently reconfirmed by high-resolution decay π^- and γ -ray spectroscopic measurements carried out by the A1 Collaboration at MAMI [9, 10] and the E13 Collaboration at J-PARC [8, 11], respectively. The extracted $J^P = 0^+$ ground state Λ -separation energies ($\mathcal{B}_{\Lambda}[0^+]$) of ${}_{\Lambda}^4\text{H}$ and ${}_{\Lambda}^4\text{He}$ are 2.157 ± 0.077 MeV and 2.39 ± 0.05 MeV, respectively, whereas those corresponding to the $J^P = 1^+$ first excited state ($\mathcal{B}_{\Lambda}[1^+]$) are 1.067 ± 0.08 MeV and 0.984 ± 0.05 MeV, respectively (cf. level scheme depicted in Fig. 1). Thus, the typical momentum scale Q associated with these single Λ -hypernuclei can be naively identified with mean binding momentum of the ground and first excited states, namely, $\bar{Q} \sim \sqrt{\mu_{\Lambda T}(\mathcal{B}_{\Lambda}[0^+] + \mathcal{B}_{\Lambda}[1^+])} \approx 50$ MeV, with $\mu_{\Lambda T} = M_{\Lambda}M_T/(M_{\Lambda} + M_T)$ being the reduced mass of these ΛT subsystems. On the other hand, the experimental binding energies (\mathcal{B}_T) of the triton and helion cores being 8.48 MeV and 7.72 MeV, respectively, the *breakdown* scale of our EFT framework may be associated with the corresponding binding momentum scale $\Lambda_H \sim \sqrt{2\mu_{dN}\mathcal{B}_T} \sim m_{\pi}$ of the cores, with μ_{dN} being the reduced mass of the deuteron (d) and nucleon (N) system, and m_{π} is the pion mass. Consequently, the expansion parameter is conservatively estimated to be at the most $\epsilon \sim \bar{Q}/m_{\pi} \lesssim \sqrt{2\mu_{\Lambda T}\mathcal{B}_{\Lambda}[0^+]}/m_{\pi} \approx 0.4$, a value reasonably small to support a valid EFT framework.

A practical computational framework for investigating three-body dynamics is thus provided by the $\not\{EFT}$ without explicit inclusion of pion. This has become a popular tool for investigating shallow bound state systems of nucleons and other hadrons (for reviews and relatively recent works, e.g., see Refs. [15, 24, 25, 44–52] and other references therein). Such a framework provides the most general approach to handle the dynamics of finely tuned systems with large scattering lengths and cross sections nearly saturating the unitary bound. This happens presumably in the vicinity of nontrivial renormalization group (RG) fixed points of the two-body contact couplings. Recently, a large number of works on $\not\{EFT}$ have appeared dealing with low-energy universal

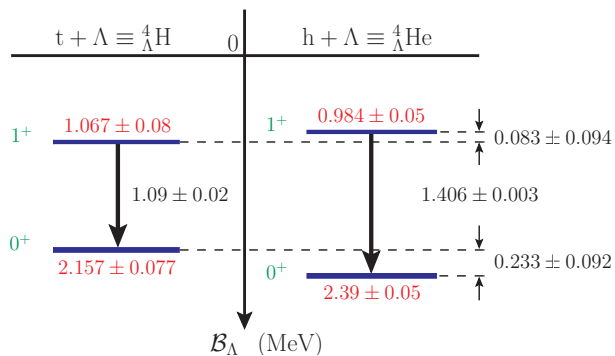


FIG. 1. Level energy (B_Λ) scheme with the ground ($J^P = 0^+$) state of ${}^4_\Lambda\text{H}$ and the first-excited ($J^P = 1^+$) states of the mirror partners (${}^4_\Lambda\text{H}$, ${}^4_\Lambda\text{He}$) taken from the recent high-resolution spectroscopic measurements at MAMI [9, 10] and J-PARC [8, 11], respectively. The ground state energy of ${}^4_\Lambda\text{He}$ on the other hand is taken from the erstwhile emulsion work of Ref. [3]. The figure is adapted from Refs. [10, 53].

physics of three-body systems. A typical signature of the onset of such universality is the appearance of a RG limit cycle resulting from the breakdown of an exact to a discrete scaling symmetry, accompanied with the emergence of a geometric tower of arbitrary shallow three-body Efimov bound states [50, 54]. In the context of hypernuclear physics, the Efimov effect and its universal role in the prediction of three-body exotic bound states have been discussed in a number of theoretical works [15, 24, 25, 51, 55] based on \mathcal{N} EFT at LO. In the ensuing analysis, we use a similar set-up to investigate whether any remnant universal feature inherent to the ΛNT system indicates Efimov-like bound state character. However, the current paucity of phenomenological information to constrain the various low-energy parameters of the theory is a major hurdle in our approach which precludes a robust prediction of the existence of Efimov-like bound states in the ${}^5_{\Lambda\Lambda}\text{H}$ and ${}^5_{\Lambda\Lambda}\text{He}$ systems. As demonstrated in our analysis, a crucial piece of information required as input to the EFT analysis is a three-body datum, namely, the three-body binding or double- Λ -separation energy $B_{\Lambda\Lambda}$ of a given mirror partner, for which there are currently no available experimental estimates. For this purpose, we rely on suitable predictions based on an existing potential models, e.g., the *ab initio* SVM analysis of Nemura *et al.* [22]. Moreover, the predictability of our halo/cluster EFT framework depends on fixing several two-body parameters from the following phenomenological information:

- the measured ground and first-excited state Λ -separation energies $B_\Lambda[J^P = 0^+, 1^+]$ of the mirror Λ -hypernuclei (${}^4_\Lambda\text{H}$, ${}^4_\Lambda\text{He}$), which we take from Refs. [3, 8–11] (cf. Fig. 1); and
- second, the value of the S -wave double- Λ scattering length $a_{\Lambda\Lambda}$, for which we consider an acceptable range of values from various phenomenological

analyses [26, 27, 35–38, 56–58], constrained by the recent RHIC data [7].

Based on these inputs, the three-body integral equations completely determine the $B_{\Lambda\Lambda}$ - $a_{\Lambda\Lambda}$ correlations for the ΛNT systems, using which preliminary estimates of the corresponding S -wave three-body scattering lengths $a_{\Lambda NT}$ are predicted. Such EFT predicted scattering lengths induce universal correlations between three-body observables, as elucidated by the so-called *Phillips-lines* [59] (cf. Fig. 10). Furthermore, for the recently suggested benchmark value, $a_{\Lambda\Lambda} = -0.80$ fm, in Ref. [26], the Λ -separation energies, $B_\Lambda({}^5_{\Lambda\Lambda}\text{H}) = 2.295$ MeV and $B_\Lambda({}^5_{\Lambda\Lambda}\text{He}) = 2.212$ MeV, are deduced.

The paper is organized as follows. In Sec. II we present the basic set-up of the \mathcal{N} EFT formalism. There we display the most general LO effective Lagrangian and the coupled system of integral equations for the ΛNT system, with appropriate scale dependent three-body contact interactions that describe RG limit cycle behavior. Section III contains our numerical results of solving the integral equations in both bound and scattering domains. In particular, through our study of the $B_{\Lambda\Lambda}$ - $a_{\Lambda\Lambda}$ correlations, we present preliminary estimates of the ΛNT scattering lengths and the corresponding Λ -separation energies. Finally, in Sec. IV we present our summary with concluding remarks. A brief discussion on the one- and two-body non-relativistic propagators in \mathcal{N} EFT is relegated to the appendix.

II. THEORETICAL FRAMEWORK

A. Effective Lagrangian

We use the theoretical framework of pionless effective field theory to investigate the bound states of the double- Λ -hypernuclear mirror systems (${}^5_{\Lambda\Lambda}\text{H}$, ${}^5_{\Lambda\Lambda}\text{He}$). In this approach the effective Lagrangian is constructed manifestly nonrelativistic on the basis of available symmetries of the relevant low-energy degrees of freedom. In our case, the explicit elementary degrees of freedom involve two Λ -hyperon *halo* fields and the generic *core* field, $T \equiv t, h$, representing one of the two mirrors (isospin) partners, namely, the triton (t) or the helion (h). In addition, it is convenient to introduce auxiliary dimer fields to unitarize and renormalize the two-body sectors [48, 50, 60–62]. Our formalism includes three such dimer fields, namely, the spin-singlet (1S_0) field $u_0 \equiv (\Lambda T)_s$, the spin-triplet (3S_1) field $u_1 \equiv (\Lambda T)_t$, and the spin-singlet $\Lambda\Lambda$ -dibaryon field $u_s \equiv (\Lambda\Lambda)_s$. Notably, these u_0 and u_1 dimer states correspond to the experimentally observed spin-singlet (0^+) ground state and spin-triplet (1^+) excited state of the mirror hypernuclei (${}^4_\Lambda\text{H}$, ${}^4_\Lambda\text{He}$) [3, 6, 8–11, 43].

The full nonrelativistic LO \mathcal{N} EFT Lagrangian can be expressed as the following string of terms:

$$\mathcal{L} = \mathcal{L}_\Lambda + \mathcal{L}_T + \mathcal{L}_{u_0} + \mathcal{L}_{u_1} + \mathcal{L}_{u_s} + \mathcal{L}_{3\text{-body}}. \quad (1)$$

The one-body Lagrangian containing the contributions of the elementary fields, namely, the Λ -hyperon and the spin-1/2 core T , is given as

$$\mathcal{L}_\Lambda = \Lambda^\dagger \left[i(v \cdot \partial) + \frac{(v \cdot \partial)^2 - \partial^2}{2M_\Lambda} + \dots \right] \Lambda, \quad (2)$$

$$\mathcal{L}_T = T^\dagger \left[i(v \cdot \partial) + \frac{(v \cdot \partial)^2 - \partial^2}{2M_T} + \dots \right] T, \quad (3)$$

where M_Λ and M_T are the respective masses of the elementary fields. Next we display the two-body parts of the Lagrangian, namely,

$$\begin{aligned} \mathcal{L}_{u_0} = & -u_0^\dagger \left[i(v \cdot \partial) + \frac{(v \cdot \partial)^2 - \partial^2}{2(M_\Lambda + M_T)} + \dots \right] u_0 \\ & - y_0 \left[u_0^\dagger \left(T^T \hat{\mathbb{P}}_{(\Lambda T)}^{(1S_0)} \Lambda \right) + \text{h.c.} \right] + \dots, \end{aligned} \quad (4)$$

$$\begin{aligned} \mathcal{L}_{u_1} = & -(u_1)_j^\dagger \left[i(v \cdot \partial) + \frac{(v \cdot \partial)^2 - \partial^2}{2(M_\Lambda + M_T)} + \dots \right] (u_1)_j \\ & - y_1 \left[(u_1)_j^\dagger \left(T^T \hat{\mathbb{P}}_{(\Lambda T)j}^{(3S_1)} \Lambda \right) + \text{h.c.} \right] + \dots, \end{aligned} \quad (5)$$

$$\begin{aligned} \mathcal{L}_{u_s} = & -u_s^\dagger \left[i(v \cdot \partial) + \frac{(v \cdot \partial)^2 - \partial^2}{4M_\Lambda} + \dots \right] u_s \\ & - y_s \left[u_s^\dagger \left(\Lambda^T \hat{\mathbb{P}}_{(\Lambda \Lambda)}^{(1S_0)} \Lambda \right) + \text{h.c.} \right] + \dots, \end{aligned} \quad (6)$$

where the spin-singlet and spin-triplet projection operators are given as

$$\begin{aligned} \hat{\mathbb{P}}_{(\Lambda \Lambda)}^{(1S_0)} &= -\frac{i}{2} \sigma_2, & \hat{\mathbb{P}}_{(\Lambda T)}^{(1S_0)} &= -\frac{i}{\sqrt{2}} \sigma_2, \\ \hat{\mathbb{P}}_{(\Lambda T)j}^{(3S_1)} &= -\frac{i}{\sqrt{2}} \sigma_2 \sigma_j, \end{aligned} \quad (7)$$

$$\mathcal{L}_{3\text{-body}}^{(A)} = -\frac{g_3^{(A)}(\Lambda_c)}{\Lambda_c^2} \left[-\frac{M_T y_0^2}{2} (u_0 \Lambda)^\dagger (u_0 \Lambda) + \frac{M_T y_0 y_1}{2} (u_0 \Lambda)^\dagger (\mathbf{u}_1 \cdot \boldsymbol{\sigma} \Lambda) - \frac{M_\Lambda y_s y_0}{\sqrt{2}} (u_0 \Lambda)^\dagger (u_s T) + \text{h.c.} \right], \quad (9)$$

$$\mathcal{L}_{3\text{-body}}^{(B)} = -\frac{g_3^{(B)}(\Lambda_c)}{\Lambda_c^2} \left[\frac{M_T y_1^2}{6} (\mathbf{u}_1 \cdot \boldsymbol{\sigma} \Lambda)^\dagger (\mathbf{u}_1 \cdot \boldsymbol{\sigma} \Lambda) + \frac{M_T y_0 y_1}{2} (\mathbf{u}_1 \cdot \boldsymbol{\sigma} \Lambda)^\dagger (u_0 \Lambda) - \frac{M_\Lambda y_s y_1}{\sqrt{2}} (\mathbf{u}_1 \cdot \boldsymbol{\sigma} \Lambda)^\dagger (u_s T) + \text{h.c.} \right]. \quad (10)$$

The regulator dependent three-body running couplings $g_3^{(A)}(\Lambda_c)$ and $g_3^{(B)}(\Lambda_c)$ which are used to absorb the scale dependence of the integral equations are *a priori* undetermined in the EFT. Hence they must be phenomenologically fixed from essential three-body data. A typical signature that Efimov physics [50, 54] is manifest in the three-body system is that the RG behavior of the three-body couplings $g_3^{(A)}$ and $g_3^{(B)}$ displays a characteristic quasi-log cyclic periodicity as a function of the regulator

with σ_j ($j = 1, 2, 3$) being the Pauli spin matrices. In the above equations $v^\mu = (1, \mathbf{0})$ is the velocity four-vector, and the couplings y_0 , y_1 , and y_s are two-body contact interactions between the respective dimer and their constituent elementary fields. Adopting to the power-counting scheme for the contact interactions apposite to finely tuned systems [44–46], these LO couplings are easily fixed as [63]

$$y_0 = y_1 = \sqrt{\frac{2\pi}{\mu_{\Lambda T}}},$$

$$\text{and} \quad y_s = \sqrt{\frac{4\pi}{M_\Lambda}}. \quad (8)$$

The ellipses in all the above Lagrangians denote subleading order terms containing four or higher derivative operators that do not contribute to our LO analysis. For pedagogical reasons a brief description of the one- and two-body nonrelativistic propagators used in the construction of the Faddeev-type coupled integral equations is presented in the appendix.

Finally, as demonstrated later in this section, since the $\Lambda\Lambda T$ three-body systems are found to exhibit RG limit cycle behavior, the set of integral equations [cf. Eqs. (11) and (12)] becomes ill-defined in the asymptotic UV limit, and a regulator, say, in the form of a sharp momentum cutoff Λ_c must be introduced to obtain regularized finite results. In that case, the basic tenet of the EFT [48] demands the introduction of non-derivatively coupled LO counterterms to renormalize the *artificial* regulator (Λ_c) dependence of the integral equations. For the $\Lambda\Lambda T$ ($J = 1/2, I = 1/2$) mirror systems, there exists two equivalent choices for the subsystem spin rearrangements that determine the elastic channels, namely, $u_0\Lambda \rightarrow u_0\Lambda$ (denoted “type-A”), and $u_1\Lambda \rightarrow u_1\Lambda$ (denoted “type-B”). With the type-A, and -B choices of the elastic channels, the three-body counterterm Lagrangians are

scale $\Lambda_c \ll \infty$. As originally suggested by Wilson [64], this unambiguously implies the onset of an RG limit cycle. Here we note that exact universality demands both three-body couplings to be identical which in principle should not depend on the details of the two-body subsystems. However, in practice, certain nominal qualitative differences do appear in the estimation of these scale dependent couplings, as seen in our results presented in the next section. This is primarily due to the specific choice

of the renormalization schemes we have adopted in the treatments of the type-A and type-B integral equations [cf. discussion below Eq. (15)]. However, such differences do not have any significant influence on the qualitative nature of the results of this work.

B. Integral equations

In Figs. 2 and 3, we display the Feynman diagrams contributing to the S -wave elastic processes, namely, $u_0\Lambda \rightarrow u_0\Lambda$ (type-A) and $u_1\Lambda \rightarrow u_1\Lambda$ (type-B), in terms of the *half-off-shell* S -wave projected amplitudes, $T_a^{(A,B)}(p, k; E)$, $T_b^{(A,B)}(p, k; E)$ and $T_c^{(A,B)}(p, k; E)$. While $T_a^{(A,B)}(p, k; E)$ denotes the elastic amplitudes, $T_b^{(A,B)}(p, k; E)$ and $T_c^{(A,B)}(p, k; E)$ are the amplitudes for the inelastic processes, $u_{0,1}\Lambda \rightarrow u_{1,0}\Lambda$ and $u_{0,1}\Lambda \rightarrow u_s\Lambda$, respectively. Here k (p) is the relative on-shell (off-shell) three-body center-of-mass mo-

mentum for the $u_{0,1} - \Lambda$ scattering processes in the initial (final) states, and $E = \mathcal{E}_{2(s,t)}^{thr} + k^2/(2\mu_{\Lambda(\Lambda T)})$ is the total center-of-mass kinetic energy measured with respect to the *three-particle breakup* threshold ($E = 0$). In other words, for each $\Lambda\Lambda T$ three-body system, there exists two *particle-dimer breakup* thresholds, viz. the deeper $\Lambda + u_0$ breakup threshold, $\mathcal{E}_{2(s)}^{thr} = -\gamma_0^2/(2\mu_{\Lambda T})$, and the shallower $\Lambda + u_1$ breakup threshold, $\mathcal{E}_{2(t)}^{thr} = -\gamma_1^2/(2\mu_{\Lambda T})$ (cf. discussions in Sec. III). Here γ_0 and γ_1 are the respective binding momenta of the singlet $u_0 \equiv (\Lambda T)_s$ and triplet $u_1 \equiv (\Lambda T)_t$ two-body subsystems, and $\mu_{\Lambda(\Lambda T)} = M_\Lambda(M_\Lambda + M_T)/(2M_\Lambda + M_T)$ is the reduced masses of the $\Lambda - (\Lambda T)_{s,t}$ three-body system. Using standard Feynman rules, the S -wave projected amplitudes for the different elastic and inelastic channels can be easily worked out. With the type-A and type-B choices of the elastic channels, the two sets of coupled integral equations for the $\Lambda\Lambda T$ mirror partners are given as [65–68]

$$\begin{aligned}
T_a^{(A)}(p, k; E) &= -\frac{1}{2}(y_0^2 M_T) \mathcal{K}_{(a)}^A(p, k; E) + \frac{M_T}{\mu_{\Lambda T}} \int_0^{\Lambda_c} \frac{dq q^2}{2\pi} \mathcal{K}_{(a)}^A(p, q, \Lambda_c; E) \mathcal{D}_0(q, E) T_a^{(A)}(q, k; E) \\
&\quad - \frac{y_0 \sqrt{3} M_T}{y_1 \mu_{\Lambda T}} \int_0^{\Lambda_c} \frac{dq q^2}{2\pi} \mathcal{K}_{(a)}^A(E; p, q) \mathcal{D}_1(q, E) T_b^{(A)}(q, k; E) + \frac{y_0 \sqrt{8}}{y_s} \int_0^{\Lambda_c} \frac{dq q^2}{2\pi} \mathcal{K}_{(b2)}^A(p, q; E) \mathcal{D}_s(q, E) T_c^{(A)}(q, k; E), \\
T_b^{(A)}(p, k; E) &= \frac{\sqrt{3}}{2}(y_0 y_1 M_T) K_{(a)}(p, k; E) - \frac{y_1 \sqrt{3} M_T}{y_0 \mu_{\Lambda T}} \int_0^{\Lambda_c} \frac{dq q^2}{2\pi} K_{(a)}(p, q; E) \mathcal{D}_0(q, E) T_a^{(A)}(q, k; E) \\
&\quad - \frac{M_T}{\mu_{\Lambda T}} \int_0^{\Lambda_c} \frac{dq q^2}{2\pi} K_{(a)}(p, q; E) \mathcal{D}_1(q, E) T_b^{(A)}(q, k; E) + \frac{y_1 \sqrt{24}}{y_s} \int_0^{\Lambda_c} \frac{dq q^2}{2\pi} K_{(b2)}(p, q; E) \mathcal{D}_s(q, E) T_c^{(A)}(q, k; E), \\
T_c^{(A)}(p, k; E) &= -\frac{1}{\sqrt{2}}(y_0 y_s M_\Lambda) K_{(b1)}(p, k; E) + \frac{y_s \sqrt{2} M_\Lambda}{y_0 \mu_{\Lambda T}} \int_0^{\Lambda_c} \frac{dq q^2}{2\pi} K_{(b1)}(p, q; E) \mathcal{D}_0(q, E) T_a^{(A)}(q, k; E) \\
&\quad + \frac{y_s \sqrt{6} M_\Lambda}{y_1 \mu_{\Lambda T}} \int_0^{\Lambda_c} \frac{dq q^2}{2\pi} K_{(b1)}(p, q; E) \mathcal{D}_1(q, E) T_b^{(A)}(q, k; E), \tag{11}
\end{aligned}$$

and,

$$\begin{aligned}
T_a^{(B)}(p, k; E) &= \frac{1}{2}(y_1^2 M_T) \mathcal{K}_{(a)}^B(p, k; E) - \frac{M_T}{\mu_{\Lambda T}} \int_0^{\Lambda_c} \frac{dq q^2}{2\pi} \mathcal{K}_{(a)}^B(p, q, \Lambda_c; E) \mathcal{D}_1(q, E) T_a^{(B)}(q, k; E) \\
&\quad - \frac{y_1 \sqrt{3} M_T}{y_0 \mu_{\Lambda T}} \int_0^{\Lambda_c} \frac{dq q^2}{2\pi} \mathcal{K}_{(a)}^B(p, q; E) \mathcal{D}_0(q, E) T_b^{(B)}(q, k; E) + \frac{y_1 \sqrt{24}}{y_s} \int_0^{\Lambda_c} \frac{dq q^2}{2\pi} \mathcal{K}_{(b2)}^B(p, q; E) \mathcal{D}_s(q, E) T_c^{(B)}(q, k; E), \\
T_b^{(B)}(p, k; E) &= \frac{\sqrt{3}}{2}(y_1 y_0 M_T) K_{(a)}(p, k; E) - \frac{y_0 \sqrt{3} M_T}{y_1 \mu_{\Lambda T}} \int_0^{\Lambda_c} \frac{dq q^2}{2\pi} K_{(a)}(p, q; E) \mathcal{D}_1(q, E) T_a^{(B)}(q, k; E) \\
&\quad + \frac{M_T}{\mu_{\Lambda T}} \int_0^{\Lambda_c} \frac{dq q^2}{2\pi} K_{(a)}(p, q; E) \mathcal{D}_0(q, E) T_b^{(B)}(q, k; E) + \frac{y_0 \sqrt{8}}{y_s} \int_0^{\Lambda_c} \frac{dq q^2}{2\pi} K_{(b2)}(p, q; E) \mathcal{D}_s(q, E) T_c^{(B)}(q, k; E), \\
T_c^{(B)}(p, k; E) &= -\sqrt{\frac{3}{2}}(y_1 y_s M_\Lambda) K_{(b1)}(p, k; E) + \frac{y_s \sqrt{6} M_\Lambda}{y_1 \mu_{\Lambda T}} \int_0^{\Lambda_c} \frac{dq q^2}{2\pi} K_{(b1)}(p, q; E) \mathcal{D}_1(q, E) T_a^{(B)}(q, k; E) \\
&\quad + \frac{y_s \sqrt{2} M_\Lambda}{y_0 \mu_{\Lambda T}} \int_0^{\Lambda_c} \frac{dq q^2}{2\pi} K_{(b1)}(p, q; E) \mathcal{D}_0(q, E) T_b^{(B)}(q, k; E), \tag{12}
\end{aligned}$$

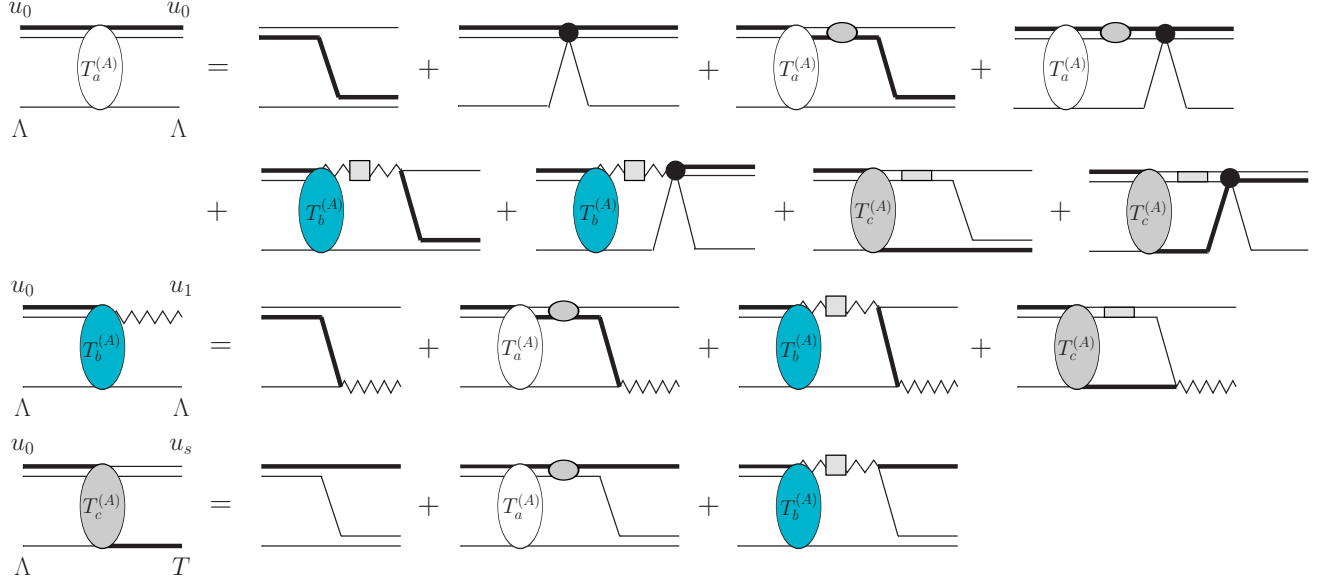


FIG. 2. Feynman diagrams for the coupled-channel integral equations, with $u_0\Lambda \rightarrow u_0\Lambda$ (type-A) choice as the elastic channel. The thin (thick) lines denote the Λ -hyperon (core $T \equiv t, h$) field propagators. The double lines denote the renormalized propagators for the spin-singlet dimer fields u_0 and u_s , and the zigzag lines denote the renormalized propagators for the spin-triplet dimer field u_1 . The dark filled circles denote the leading order three-body contact interactions, while the oval, and rectangular gray blobs represent dressings of the dimer propagators with resummed loops (cf. discussion in the appendix).

respectively, where in the above equations the two-body couplings y_0 , y_1 , and y_s are determined by using Eq. (8). The S -wave projected two-point Green's functions (cf. Eq. (37) in the appendix), namely,

$$\begin{aligned} \mathcal{D}_0(q, E) &= \frac{1}{\gamma_0 - \sqrt{q^2 \frac{\mu_{\Lambda T}}{\mu_{\Lambda(\Lambda T)}} - 2\mu_{\Lambda T}E - i\eta - i\eta}}, \\ \mathcal{D}_1(q, E) &= \frac{1}{\gamma_1 - \sqrt{q^2 \frac{\mu_{\Lambda T}}{\mu_{\Lambda(\Lambda T)}} - 2\mu_{\Lambda T}E - i\eta - i\eta}}, \\ \mathcal{D}_s(q, E) &= \frac{1}{\frac{1}{a_{\Lambda\Lambda}} - \sqrt{q^2 \frac{M_\Lambda}{2\mu_{T(\Lambda\Lambda)}} - M_\Lambda E - i\eta - i\eta}}, \end{aligned} \quad (13)$$

contain the contributions of the u_0 , u_1 , and u_s intermediate dimer states, with $\mu_{T(\Lambda\Lambda)} = (2M_\Lambda M_T)/(2M_\Lambda + M_T)$, which is the reduced mass of the T - $(\Lambda\Lambda)_s$ three-body system. The T -exchange interaction kernel $K_{(a)}$, and the two possible Λ -exchange interaction kernels, $K_{(b1)}$ and $K_{(b2)}$, can be expressed as

$$K_{(a)}(p, \kappa; E) = \frac{1}{2p\kappa} \ln \left[\frac{p^2 + \kappa^2 + \frac{2\mu_{\Lambda T}}{M_T} p\kappa - 2\mu_{\Lambda T}E}{p^2 + \kappa^2 - \frac{2\mu_{\Lambda T}}{M_T} p\kappa - 2\mu_{\Lambda T}E} \right],$$

and

$$\begin{aligned} K_{(b1)}(p, \kappa; E) &= \frac{1}{2p\kappa} \ln \left[\frac{\frac{M_\Lambda}{2\mu_{\Lambda T}} p^2 + \kappa^2 + p\kappa - M_\Lambda E}{\frac{M_\Lambda}{2\mu_{\Lambda T}} p^2 + \kappa^2 - p\kappa - M_\Lambda E} \right], \\ K_{(b2)}(p, \kappa; E) &= \frac{1}{2p\kappa} \ln \left[\frac{p^2 + \frac{M_\Lambda}{2\mu_{\Lambda T}} \kappa^2 + p\kappa - M_\Lambda E}{p^2 + \frac{M_\Lambda}{2\mu_{\Lambda T}} \kappa^2 - p\kappa - M_\Lambda E} \right], \end{aligned} \quad (14)$$

respectively, where the generic momentum $\kappa = k(q)$ denotes the on-shell (loop) momenta. The inclusion of the regulator-dependent (Λ_c -dependent) three-body contact couplings $g_3^{(A,B)}(\Lambda_c)$ modifies the one-particle exchange interaction kernels, $K_{(a)}$ and $K_{(b2)}$, in the respective elastic channels as:

$$\begin{aligned} \mathcal{K}_{(a)}^{A,B}(p, \kappa, \Lambda_c; E) &= \left[K_{(a)}(p, \kappa; E) - \frac{g_3^{(A,B)}(\Lambda_c^2)}{\Lambda_c^2} \right], \\ \mathcal{K}_{(b2)}^{A,B}(p, \kappa, \Lambda_c; E) &= \left[K_{(b2)}(p, \kappa; E) - \frac{g_3^{(A,B)}(\Lambda_c^2)}{\Lambda_c^2} \right]. \end{aligned} \quad (15)$$

Here we point out that in this work we used a minimal prescription of introducing the scale dependent three-body couplings only in the elastic channels. In general, the most systematic method of renormalization is to include them in all the inelastic channels as well, e.g., as done in Refs. [15, 55]. In the present case we find that the latter method leads to certain uncontrollable numerical instabilities in determining the limit cycle behaviors of $g_3^{(A,B)}(\Lambda_c)$. This is perhaps due to the simultaneous admixture of the negative $(\Lambda\Lambda)_s$ and positive $(\Lambda T)_{s,t}$ two-body scattering lengths associated with the virtual and real bound state dimers, respectively. Hence, we took recourse to the former simplistic prescription. Either way, since these unknown scale dependent three-body couplings are needed to be fixed phenomenologically during evaluations of the integral equations, they are expected to get accordingly renormalized in the different coupled channels. Thereby, the essential qualitative features of

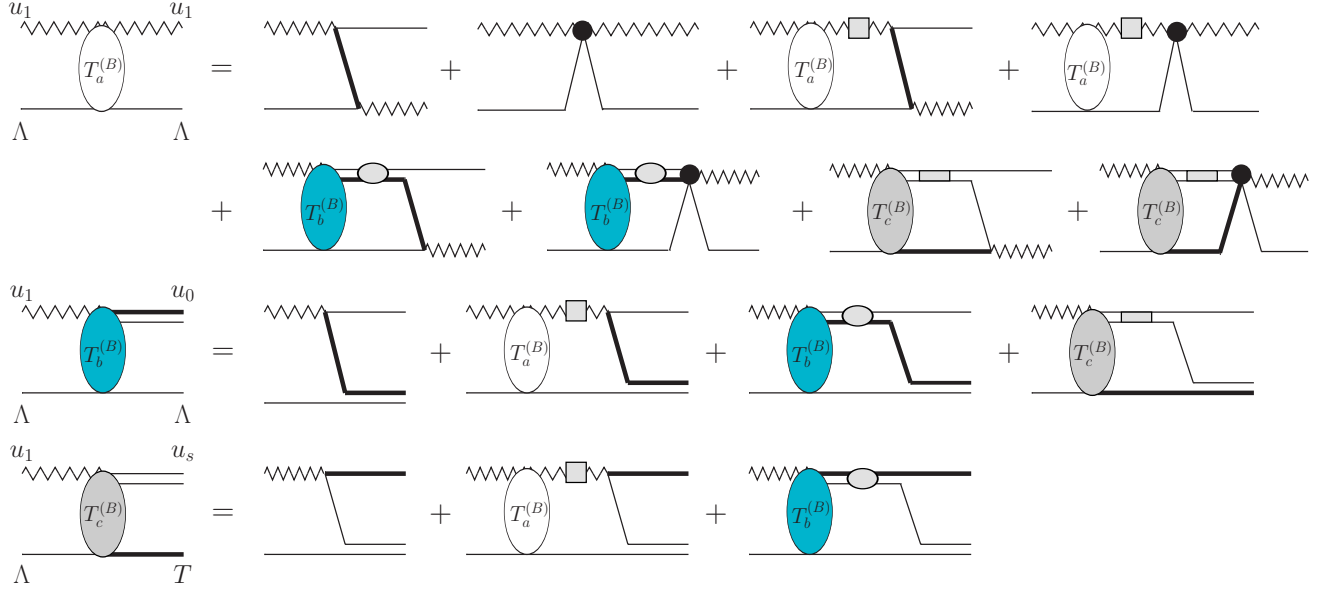


FIG. 3. Feynman diagrams for the coupled-channel integral equations, with $u_1\Lambda \rightarrow u_1\Lambda$ (type-B) choice for the elastic channel. The thin (thick) lines denote the Λ -hyperon (core $T \equiv t, h$) field propagators. The double lines denote the renormalized propagators for the spin-singlet dimer fields u_0 and u_s , and the zigzag lines denote the renormalized propagators for the spin-triplet dimer field u_1 . The dark filled circles denote the leading order three-body contact interactions, while the square, oval, and rectangular gray blobs represent dressings of the dimer propagators with resummed loops (cf. discussion in the appendix).

our investigations of the three-body bound states (e.g., the quasiperiodicity of the RG limit cycle) are by and large expected to remain unaffected. This issue is elucidated later in our results presented in the forthcoming section.

C. Three-body scattering lengths

The coupled integral equations displayed in the previous subsection must be renormalized and then solved numerically to yield predictions for the $\Lambda\Lambda T$ three-body scattering amplitudes. For a given on-shell relative momentum $k = |\mathbf{k}|$ and three-body center-of-mass kinetic energy E , the kinematical scattering domain lies between the particle-dimer breakup thresholds $\mathcal{E}_{2(s,t)}^{thr}$ and the three-particle breakup threshold, i.e., $\mathcal{E}_{2(s,t)}^{thr} < E < 0$. In contrast with the kinematical domain of three-body bound states ($E < \mathcal{E}_{2(s,t)}^{thr}$) with imaginary k free of singularities, the integral equations in the scatter-

ing domain develop singularities associated with poles of the $(\Lambda T)_{s,t}$ -dimer propagators $\mathcal{D}_{0,1}(q, E)$ for certain values of the loop momenta q . For the type-A integral equations the only poles are those that arise from the $\mathcal{D}_0(q, E)$ propagator insertions at $q = k$. While for the type-B integral equations poles arise due to the insertions of both $(\Lambda T)_{s,t}$ -dimer propagators, namely, $\mathcal{D}_1(q, E)$ has a pole at $q = k$ and $\mathcal{D}_0(q, E)$ has a pole at $q = \sqrt{k^2 + (\gamma_0^2 - \gamma_1^2)(\mu_{\Lambda(\Lambda T)}/\mu_{\Lambda T})}$. To avoid these poles, a *principal value* prescription must be applied in the appropriate loop integrals to extract the three-body scattering amplitudes. Furthermore, it is numerically advantageous to express the otherwise complex-valued integral equations below the three-particle breakup threshold in terms of the real-valued renormalized K -matrix elements $\mathbb{K}_{a,b,c}^{(A,B)}(p, k; E)$ for the respective choice of the elastic processes, viz. $u_{(0,1)}\Lambda \rightarrow u_{(0,1)}\Lambda$. To this end we display the principal value prescription modified renormalized K -matrix integral equations:

$$\begin{aligned} \mathbb{K}_a^{(A)}(p, k; E) &= -\frac{M_T}{4\mu_{\Lambda T}} \mathcal{M}_{(a)}^{A(0)}(p, k; E) - \frac{M_T}{2\pi\mu_{\Lambda T}} \mathcal{P} \int_0^{\Lambda_c} dq \mathcal{M}_{(a)}^{A(0)}(p, q, \Lambda_c; E) \frac{q^2}{q^2 - k^2} \mathbb{K}_a^{(A)}(q, k; E) \\ &+ \frac{\sqrt{3}M_T y_0}{2\pi\mu_{\Lambda T} y_1} \int_0^{\Lambda_c} dq \mathcal{M}_{(a)}^{A(0)}(p, q, \Lambda_c; E) \frac{q^2}{q^2 - k^2 + \frac{\mu_{\Lambda(\Lambda T)}}{\mu_{\Lambda T}}(\gamma_0^2 - \gamma_1^2)} \mathbb{K}_b^{(A)}(q, k; E) \\ &- \frac{\sqrt{2}}{\pi} \frac{y_0}{y_s} \mathcal{P} \int_0^{\Lambda_c} dq \mathcal{M}_{(b2)}^{A(0)}(p, q, \Lambda_c; E) \frac{q^2}{q^2 - k^2} \mathbb{K}_c^{(A)}(q, k; E), \end{aligned}$$

$$\begin{aligned}
\mathbb{K}_b^{(A)}(p, k; E) &= \frac{\sqrt{3}M_T y_1}{4\mu_{\Lambda T} y_0} M_{(a)}^{(1)}(p, k; E) + \frac{\sqrt{3}M_T y_1}{2\pi\mu_{\Lambda T} y_0} \mathcal{P} \int_0^{\Lambda_c} dq M_{(a)}^{(1)}(p, q; E) \frac{q^2}{q^2 - k^2} \mathbb{K}_a^{(A)}(q, k; E) \\
&\quad + \frac{M_T}{2\pi\mu_{\Lambda T}} \int_0^{\Lambda_c} dq M_{(a)}^{(1)}(p, q; E) \frac{q^2}{q^2 - k^2 + \frac{\mu_{\Lambda(\Lambda T)}}{\mu_{\Lambda T}}(\gamma_0^2 - \gamma_1^2)} \mathbb{K}_b^{(A)}(q, k; E) \\
&\quad - \frac{\sqrt{6}}{\pi} \frac{y_1}{y_s} \mathcal{P} \int_0^{\Lambda_c} dq M_{(b2)}^{(1)}(p, q; E) \frac{q^2}{q^2 - k^2} \mathbb{K}_c^{(A)}(q, k; E), \\
\mathbb{K}_c^{(A)}(p, k; E) &= \frac{M_\Lambda}{2\sqrt{2}\mu_{\Lambda T} y_0} M_{(b1)}(p, k; E) + \frac{M_\Lambda}{\sqrt{2}\pi\mu_{\Lambda T} y_0} \mathcal{P} \int_0^{\Lambda_c} dq M_{(b1)}(p, q; E) \frac{q^2}{q^2 - k^2} \mathbb{K}_a^{(A)}(q, k; E) \\
&\quad + \sqrt{\frac{3}{2}} \frac{M_\Lambda}{\pi\mu_{\Lambda T} y_1} \int_0^{\Lambda_c} dq M_{(b1)}(p, q; E) \frac{q^2}{q^2 - k^2 + \frac{\mu_{\Lambda(\Lambda T)}}{\mu_{\Lambda T}}(\gamma_0^2 - \gamma_1^2)} \mathbb{K}_b^{(A)}(q, k; E),
\end{aligned} \tag{16}$$

for the type-A elastic channel with $E \equiv E_A = \mathcal{E}_{2(s)}^{thr} + k^2/(2\mu_{\Lambda(\Lambda T)})$, and

$$\begin{aligned}
\mathbb{K}_a^{(B)}(p, k; E) &= \frac{M_T}{4\mu_{\Lambda T}} \mathcal{M}_{(a)}^{B(1)}(p, k; E) + \frac{M_T}{2\pi\mu_{\Lambda T}} \mathcal{P} \int_0^{\Lambda_c} dq \mathcal{M}_{(a)}^{B(1)}(p, q, \Lambda_c; E) \frac{q^2}{q^2 - k^2} \mathbb{K}_a^{(B)}(q, k; E) \\
&\quad + \frac{\sqrt{3}M_T y_1}{2\pi\mu_{\Lambda T} y_0} \mathcal{P} \int_0^{\Lambda_c} dq \mathcal{M}_{(a)}^{B(1)}(p, q, \Lambda_c; E) \frac{q^2}{q^2 - k^2 - \frac{\mu_{\Lambda(\Lambda T)}}{\mu_{\Lambda T}}(\gamma_0^2 - \gamma_1^2)} \mathbb{K}_b^{(B)}(q, k; E) \\
&\quad - \frac{\sqrt{6}}{\pi} \frac{y_1}{y_s} \mathcal{P} \int_0^{\Lambda_c} dq \mathcal{M}_{(b2)}^{B(1)}(p, q, \Lambda_c; E) \frac{q^2}{q^2 - k^2} \mathbb{K}_c^{(B)}(q, k; E), \\
\mathbb{K}_b^{(B)}(p, k; E) &= \frac{\sqrt{3}M_T y_0}{4\mu_{\Lambda T} y_1} M_{(a)}^{(0)}(p, k; E) + \frac{\sqrt{3}M_T y_0}{2\pi\mu_{\Lambda T} y_1} \mathcal{P} \int_0^{\Lambda_c} dq M_{(a)}^{(0)}(p, q; E) \frac{q^2}{q^2 - k^2} \mathbb{K}_a^{(B)}(q, k; E) \\
&\quad - \frac{M_T}{2\pi\mu_{\Lambda T}} \mathcal{P} \int_0^{\Lambda_c} dq M_{(a)}^{(0)}(p, q; E) \frac{q^2}{q^2 - k^2 - \frac{\mu_{\Lambda(\Lambda T)}}{\mu_{\Lambda T}}(\gamma_0^2 - \gamma_1^2)} \mathbb{K}_b^{(B)}(q, k; E) \\
&\quad - \frac{\sqrt{2}}{\pi} \frac{y_0}{y_s} \mathcal{P} \int_0^{\Lambda_c} dq M_{(b2)}^{(0)}(p, q; E) \frac{q^2}{q^2 - k^2} \mathbb{K}_c^{(B)}(q, k; E), \\
\mathbb{K}_c^{(B)}(p, k; E) &= \frac{\sqrt{3}M_\Lambda y_s}{2\sqrt{2}\mu_{\Lambda T} y_1} M_{(b1)}(p, k; E) + \sqrt{\frac{3}{2}} \frac{M_\Lambda y_s}{\pi\mu_{\Lambda T} y_1} \mathcal{P} \int_0^{\Lambda_c} dq M_{(b1)}(p, q; E) \frac{q^2}{q^2 - k^2} \mathbb{K}_a^{(B)}(q, k; E) \\
&\quad + \frac{M_\Lambda}{\sqrt{2}\pi\mu_{\Lambda T} y_0} \mathcal{P} \int_0^{\Lambda_c} dq M_{(b1)}(p, q; E) \frac{q^2}{q^2 - k^2 - \frac{\mu_{\Lambda(\Lambda T)}}{\mu_{\Lambda T}}(\gamma_0^2 - \gamma_1^2)} \mathbb{K}_b^{(B)}(q, k; E),
\end{aligned} \tag{17}$$

for the type-B elastic channel with $E \equiv E_B = \mathcal{E}_{2(t)}^{thr} + k^2/(2\mu_{\Lambda(\Lambda T)})$. The symbol “ \mathcal{P} ” stands for a principal value integral which involves rewriting the complex-valued dimer propagators with $i\eta$ prescription in terms of real-valued propagators, namely,

$$\frac{1}{q^2 - k^2 - i\eta} = \mathcal{P} \frac{1}{q^2 - k^2} + i\pi\delta(q^2 - k^2),$$

and

$$\begin{aligned}
&\frac{1}{q^2 - k^2 - \frac{\mu_{\Lambda(\Lambda T)}}{\mu_{\Lambda T}}(\gamma_0^2 - \gamma_1^2) - i\eta} \\
&= \mathcal{P} \frac{1}{q^2 - k^2 - \frac{\mu_{\Lambda(\Lambda T)}}{\mu_{\Lambda T}}(\gamma_0^2 - \gamma_1^2)} \\
&\quad + i\pi\delta\left(q^2 - k^2 - \frac{\mu_{\Lambda(\Lambda T)}}{\mu_{\Lambda T}}(\gamma_0^2 - \gamma_1^2)\right).
\end{aligned}$$

The S -wave projected Λ and T -exchange interactions kernels in this case are rewritten as:

$$\begin{aligned}
M_{(a)}^{(0,1)}(p, \kappa; E) &= \left(\frac{\mu_{\Lambda T}}{\mu_{\Lambda T}} \right) K_{(a)}(p, \kappa; E) \\
&\quad \times \left(\gamma_{0,1} + \sqrt{p^2 \frac{\mu_{\Lambda T}}{\mu_{\Lambda(\Lambda T)}} - 2\mu_{\Lambda T} E} \right), \\
M_{(b1)}(p, \kappa; E) &= K_{(b1)}(p, \kappa; E) \\
&\quad \times \left(\frac{p^2 - k^2}{\frac{1}{a_{\Lambda\Lambda}} - \sqrt{p^2 \frac{M_{\Lambda}}{2\mu_{T(\Lambda\Lambda)}} - M_{\Lambda} E}} \right), \\
M_{(b2)}^{(0,1)}(p, \kappa; E) &= \left(\frac{\mu_{\Lambda(\Lambda T)}}{\mu_{\Lambda T}} \right) K_{(b2)}(p, \kappa; E) \\
&\quad \times \left(\gamma_{0,1} + \sqrt{p^2 \frac{\mu_{\Lambda T}}{\mu_{\Lambda(\Lambda T)}} - 2\mu_{\Lambda T} E} \right), \tag{18}
\end{aligned}$$

and the corresponding three-body force modified Λ_c dependent kernels needed are:

$$\begin{aligned}
\mathcal{M}_{(a)}^{A,B(0,1)}(p, \kappa, \Lambda_c; E) &= \left(\frac{\mu_{\Lambda(\Lambda T)}}{\mu_{\Lambda T}} \right) \mathcal{K}_{(a)}^{A,B}(p, \kappa, \Lambda_c; E) \\
&\quad \times \left(\gamma_{0,1} + \sqrt{p^2 \frac{\mu_{\Lambda T}}{\mu_{\Lambda(\Lambda T)}} - 2\mu_{\Lambda T} E} \right), \\
\mathcal{M}_{(b2)}^{A,B(0,1)}(p, \kappa, \Lambda_c; E) &= \left(\frac{\mu_{\Lambda(\Lambda T)}}{\mu_{\Lambda T}} \right) \mathcal{K}_{(b2)}^{A,B}(p, \kappa, \Lambda_c; E) \\
&\quad \times \left(\gamma_{0,1} + \sqrt{p^2 \frac{\mu_{\Lambda T}}{\mu_{\Lambda(\Lambda T)}} - 2\mu_{\Lambda T} E} \right), \tag{19}
\end{aligned}$$

where $\kappa = k(q)$ is the on-shell (loop) momentum. In the above integral equations, the unrenormalized complex-valued amplitudes $T_a^{(A,B)}(p, k; E)$ are related to the renormalized real-valued K -matrix elements $\mathbb{K}_{a,b,c}^{(A,B)}(p, k; E)$ by the following relations:

$$\begin{aligned}
\frac{\mathbb{K}_a^{(A)}(p, k; E)}{k^2 - p^2} &= \left(\frac{\mu_{\Lambda T}}{4\pi\gamma_0} \right) \frac{\sqrt{Z_0} T_a^{(A)}(p, k; E) \sqrt{Z_0}}{\gamma_0 - \sqrt{q^2 \frac{\mu_{\Lambda T}}{\mu_{\Lambda(\Lambda T)}} - 2\mu_{\Lambda T} E}}, \\
\frac{\mathbb{K}_b^{(A)}(p, k; E)}{k^2 - p^2 - \frac{\mu_{\Lambda(\Lambda T)}}{\mu_{\Lambda T}}(\gamma_0^2 - \gamma_1^2)} &= \left(\frac{\mu_{\Lambda T}}{4\pi\gamma_0} \right) \frac{\sqrt{Z_0} T_b^{(A)}(p, k; E) \sqrt{Z_0}}{\gamma_1 - \sqrt{q^2 \frac{\mu_{\Lambda T}}{\mu_{\Lambda(\Lambda T)}} - 2\mu_{\Lambda T} E}}, \\
\frac{\mathbb{K}_c^{(A)}(p, k; E)}{k^2 - p^2} &= \left(\frac{\mu_{\Lambda T}}{4\pi\gamma_0} \right) \frac{\sqrt{Z_0} T_c^{(A)}(p, k; E) \sqrt{Z_0}}{\frac{1}{a_{\Lambda\Lambda}} - \sqrt{q^2 \frac{M_{\Lambda}}{2\mu_{T(\Lambda\Lambda)}} - M_{\Lambda} E}}, \tag{20}
\end{aligned}$$

for the type-A amplitudes, and

$$\frac{\mathbb{K}_a^{(B)}(p, k; E)}{k^2 - p^2} = \left(\frac{\mu_{\Lambda T}}{4\pi\gamma_1} \right) \frac{\sqrt{Z_1} T_a^{(B)}(p, k; E) \sqrt{Z_1}}{\gamma_1 - \sqrt{q^2 \frac{\mu_{\Lambda T}}{\mu_{\Lambda(\Lambda T)}} - 2\mu_{\Lambda T} E}},$$

$$\begin{aligned}
\frac{\mathbb{K}_b^{(B)}(p, k; E)}{k^2 - p^2 + \frac{\mu_{\Lambda(\Lambda T)}}{\mu_{\Lambda T}}(\gamma_0^2 - \gamma_1^2)} &= \left(\frac{\mu_{\Lambda T}}{4\pi\gamma_1} \right) \frac{\sqrt{Z_1} T_b^{(B)}(p, k; E) \sqrt{Z_1}}{\gamma_0 - \sqrt{q^2 \frac{\mu_{\Lambda T}}{\mu_{\Lambda(\Lambda T)}} - 2\mu_{\Lambda T} E}}, \\
\frac{\mathbb{K}_c^{(B)}(p, k; E)}{k^2 - p^2} &= \left(\frac{\mu_{\Lambda T}}{4\pi\gamma_1} \right) \frac{\sqrt{Z_1} T_c^{(B)}(p, k; E) \sqrt{Z_1}}{\frac{1}{a_{\Lambda\Lambda}} - \sqrt{q^2 \frac{M_{\Lambda}}{2\mu_{T(\Lambda\Lambda)}} - M_{\Lambda} E}}, \tag{21}
\end{aligned}$$

for the type-B amplitudes, where $Z_{0,1}$ are the $u_{0,1}$ -dimer field wave function renormalization constants, defined as the residues of the renormalized dressed dimer propagators $\Delta_{0,1}(k_0, \mathbf{k})$ [cf. Eq. (37) in the appendix]:

$$\begin{aligned}
Z_0^{-1} &= \frac{d[\Delta_0^{-1}(k_0, \mathbf{0})]}{dk_0} \Big|_{k_0 = -B_{\Lambda}[0^+]} = \frac{\mu_{\Lambda T}^2 y_0^2}{2\pi\gamma_0}, \\
Z_1^{-1} &= \frac{d[\Delta_1^{-1}(k_0, \mathbf{0})]}{dk_0} \Big|_{k_0 = -B_{\Lambda}[1^+]} = \frac{\mu_{\Lambda T}^2 y_1^2}{2\pi\gamma_1}. \tag{22}
\end{aligned}$$

Finally, the $J = 1/2$ S -wave $\Lambda\Lambda T$ scattering lengths corresponding to the constituent spin-singlet and spin-triplet ΛT subsystems are obtained by numerically solving the above K -matrix equations for the renormalized on-shell elastic-scattering amplitudes $\mathbb{K}_a^{(A,B)}(k, k)$, and then taking the threshold limit according to the definition

$$a_{3(s,t)} = - \lim_{k \rightarrow 0} \mathbb{K}_a^{(A,B)}(k, k). \tag{23}$$

It is notable that neither of the two three-body scattering lengths $a_{3(s,t)}$ can be considered as physical observables. On the other hand, albeit practical difficulties, it may not be on the whole impossible to extract the effective three-body scattering length $a_{\Lambda\Lambda T}$ at low-energies from the $(2J+1)$ -spin averaged S -wave elastic cross section $\sigma_{\Lambda\Lambda T}^{el}$ by using the relation

$$a_{\Lambda\Lambda T} = \sqrt{\frac{1}{4} a_{3(s)}^2 + \frac{3}{4} a_{3(t)}^2}, \tag{24}$$

vis-a-vis, the prescription:

$$\begin{aligned}
\sigma_{\Lambda\Lambda T}^{el} &= \frac{1}{4} \sigma_{3(s)}(\text{type-A}) + \frac{3}{4} \sigma_{3(t)}(\text{type-B}); \\
a_{3(s,t)} &= \lim_{k \rightarrow 0} \sqrt{\frac{1}{4\pi} \sigma_{3(s,t)}(\text{type-A,B})}, \\
a_{\Lambda\Lambda T} &= \lim_{k \rightarrow 0} \sqrt{\frac{1}{4\pi} \sigma_{\Lambda\Lambda T}^{el}}. \tag{25}
\end{aligned}$$

Thus, our EFT framework provides a viable prescription to determine the three-body scattering lengths via numerical solutions to the renormalized K -matrix integral equations. Having said that it must be borne in mind that as yet there exists no experimental facility capable of extracting these scattering lengths by measuring the above elastic cross sections. The unstable nature of the

Λ -hyperon poses immense technical challenges to be used either as targets or projectiles in scattering experiments. Nevertheless, the purpose of the present exercise is to demonstrate the kind of prototypical analysis that may be necessary whenever such information becomes available from future experimental investigations.

D. Asymptotic bound state analysis

In the investigation of three-body bound state characteristic in the $\Lambda\Lambda T$ cluster systems, the emergence of RG limit-cycle behavior could be easily checked by studying the UV limit of the coupled integral equations where the off-shell or loop momenta is asymptotically large, i.e., $q, p \sim \Lambda_c \rightarrow \infty$, while the on-shell energy and relative momenta is small, i.e., $E, k \sim \gamma_{0,1} \sim 1/a_{\Lambda\Lambda} \ll p, q$. In this limit the inhomogeneous parts as well as the Λ_c^{-2} suppressed three-body contributions to the integral equations drop out. After suitable redefinitions of the half-off-shell amplitudes, they may be shown to scale for generic off-shell asymptotic momenta κ as $T_{a,b,c}^{(A,B)}(\kappa \rightarrow \infty) \sim \kappa^{s-1}$. Finally through a sequence of *Mellin transformations*, both sets of integral equations reduce to same transcendental form:

$$1 = \left(\frac{M_T}{2\pi\mu_{\Lambda T}C_1} \right) \left[\frac{2\pi \sin[s \sin^{-1}(a/2)]}{s \cos[\pi s/2]} \right] + \left(\frac{M_\Lambda}{\pi^2\mu_{\Lambda T}C_1C_2} \right) \left[\frac{2\pi \sin[s \cot^{-1}\sqrt{4b-1}]}{s \cos[\pi s/2]} \right]^2, \quad (26)$$

where

$$a = \frac{2\mu_{\Lambda T}}{M_T}, \quad b = \frac{M_\Lambda}{2\mu_{\Lambda T}}, \\ C_1 = \sqrt{\frac{\mu_{\Lambda T}}{\mu_{\Lambda(\Lambda T)}}}, \quad C_2 = \sqrt{\frac{M_\Lambda}{2\mu_{T(\Lambda\Lambda)}}}.$$

Solving for the exponent s in above equation yields the following imaginary values:

$$s = \pm i s_0^\infty \begin{cases} s_0^\infty = 1.03517\dots & \text{for } {}^5_{\Lambda\Lambda}\text{H} \\ s_0^\infty = 1.03516\dots & \text{for } {}^5_{\Lambda\Lambda}\text{He}. \end{cases} \quad (27)$$

The small numerical difference between the values of the asymptotic limit cycle parameter s_0^∞ reflects their universal character with reasonably good isospin symmetry in the three-body sector. The imaginary solutions can be formally attributed to the existence of Efimov states in the *unitary limit* of the two mirror $\Lambda\Lambda T$ clusters and parametrize the onset of discrete scaling invariance. A detailed exposition of this kind of asymptotic analysis leading to the Efimov effect is found in Ref. [50]. In the next section we present a qualitative assay of our numerical results for the nonasymptotic solutions to the integral equations and their possible implications in the low-energy domain.

Particle	Symbol	Mass (MeV)	Binding energy (MeV)
Λ -hyperon	Λ	1115.683	-
Triton ${}^3\text{H}$	t	2808.921	8.48
Helion ${}^3\text{He}$	h	2808.391	7.72

TABLE I. Particle data used in our calculations [69].

III. RESULTS AND DISCUSSION

For our numerical evaluations, we use the masses of the particles as displayed in Table. I. As a comparison with our already obtained asymptotic limit cycle parameter s_0^∞ for each mirror hypernuclei, the analogous nonasymptotic parameter s_0 may be obtained by studying the RG behavior of the three-body couplings $g_3^{(A,B)}(\Lambda_c)$ for nonasymptotic kinematics. The s_0 parameter is, however, nonuniversal in character and sensitive to the cut-off variations. Nevertheless, it may be shown that as $\Lambda_c \rightarrow \infty$, $s_0 \rightarrow s_0^\infty$ [52]. We note that currently there is no empirical three-body information available to constraint $g_3^{(A,B)}$. Thus, we adopt a strategy similar to the earlier pursued works [24, 25, 52]. We assume that ${}^5_{\Lambda\Lambda}\text{H}$ and ${}^5_{\Lambda\Lambda}\text{He}$ already form Efimov-like bound cluster states and thereby investigate the RG of $g_3^{(A,B)}$ by choosing two sets of values of the three-body binding or double- Λ -separation energies¹ ($B_{\Lambda\Lambda}$) for the mirror partners, predicted by the *ab initio* coupled channel potential model of Nemura *et al.* [22] using SVM analysis (cf. Table. II). These predictions correspond to the two representative S -wave double- Λ scattering lengths, namely, $a_{\Lambda\Lambda} = -0.91$ and -1.37 fm, taken from the old Nijmegen hard-core potential models, mND_S and ND_S, respectively, of Ref. [56], but consistent with the constraints based on recent theoretical analyses [36–38] based on RHIC data [7].

In Fig. 4 we demonstrate the cutoff regulator dependence of the three-body coupling $g_3^{(A,B)}(\Lambda_c)$ for the $\Lambda\Lambda T$

¹ The double- Λ -separation energy $B_{\Lambda\Lambda}$, as commonly referred to in the context of potential model analyses, is interpreted in our EFT framework as the three-body eigenenergy, $-E = B_{\Lambda\Lambda}$, obtained as the likely ground-state solution to the homogeneous part of the integral equations. Additionally, in the cluster model framework it is conventional to define an *incremental binding energy* $\Delta B_{\Lambda\Lambda}$ which is related to $B_{\Lambda\Lambda}$ (measured with respect to the $\Lambda\Lambda T$ three-particle breakup threshold) as [16]

$$\Delta B_{\Lambda\Lambda} = B_{\Lambda\Lambda} - 2\mathcal{B}_\Lambda^{avg}, \quad (28)$$

where,

$$\mathcal{B}_\Lambda^{avg} = \frac{1}{4}\mathcal{B}_\Lambda[0^+] + \frac{3}{4}\mathcal{B}_\Lambda[1^+], \quad (29)$$

is the $(2J+1)$ *spin averaged* Λ -separation energy of the singlet and triplet two-body subsystems (interpreted in the EFT as the $(\Lambda T)_{s,t}$ subsystem averaged binding energy). Thus, the predicted values of $B_{\Lambda\Lambda}$ from past *ab initio* potential model analysis, such as in Ref. [22], may be used to supplant the old results of $\Delta B_{\Lambda\Lambda}$ by reevaluating them using the recent experimental inputs for the Λ -separation energies of the ground (singlet) and first (triplet) excited states of the (${}^4_\Lambda\text{H}$, ${}^4_\Lambda\text{He}$) mirrors [8–11].

$\Lambda\Lambda$ -Hypernuclear mirror (a, b) Sets	S -wave $\Lambda\Lambda$ Scattering length $a_{\Lambda\Lambda}$ (fm)	$\Lambda\Lambda$ -Separation energy $B_{\Lambda\Lambda}$ (MeV) [22]	Incremental binding energy $\Delta B_{\Lambda\Lambda}$ (MeV) reevaluated (this work)	Critical cutoff $\Lambda_{\text{crit}}^{(n=0)}$ (MeV) (with $g_3^{(A,B)} = 0$)	cutoff $\Lambda_{\text{pot}}^{(n=0)}$ (MeV) (with $g_3^{(A,B)} = 0$)
Ia (${}_{\Lambda\Lambda}^5\text{H}$)	-0.91 (mND _S) [56]	3.750	1.071	235.028	437.654
Ib (${}_{\Lambda\Lambda}^5\text{He}$)	-0.91 (mND _S) [56]	3.660	0.989	269.621	429.833
IIa (${}_{\Lambda\Lambda}^5\text{H}$)	-1.37 (ND _S) [56]	4.050	1.381	205.448	403.285
IIb (${}_{\Lambda\Lambda}^5\text{He}$)	-1.37 (ND _S) [56]	3.960	1.289	234.522	396.332

TABLE II. Two sets of predictions for the three-body binding or double- Λ -separation energy $B_{\Lambda\Lambda}$ for the (${}_{\Lambda\Lambda}^5\text{H}$, ${}_{\Lambda\Lambda}^5\text{He}$) mirrors using the coupled-channel potential model SVM analysis of Nemura *et al.* [22]. The corresponding double- Λ scattering lengths used are two representative values based on the old Nijmegen hard-core potential models [56] (names in parentheses) consistent with the currently accepted range, $-1.92 \text{ fm} \lesssim a_{\Lambda\Lambda} \lesssim -0.5 \text{ fm}$ [36–38], as constrained by the recent RHIC data [7]. The values of the incremental binding energies $\Delta B_{\Lambda\Lambda}$ are obtained utilizing the recent experimental input for the Λ -separation energies of the ground (singlet) and first (triplet) excited states of the (${}_{\Lambda}^4\text{H}$, ${}_{\Lambda}^4\text{He}$) mirrors [8–11]. Furthermore, with the three-body contact interactions excluded from our integral equations, the critical cutoffs, $\Lambda_c = \Lambda_{\text{crit}}^{(n=0)}$ (see text), associated with the ground ($n = 0$) state Efimov-like trimers for each mirror double- Λ -hypernuclei, are also displayed. The rightmost column shows our adjusted cutoff values, $\Lambda_c = \Lambda_{\text{pot}}^{(n=0)}$, which reproduce the above values of $B_{\Lambda\Lambda}$ as ground state eigenenergies. The paired ($B_{\Lambda\Lambda}$, $a_{\Lambda\Lambda}$) data points for cases Ia and Ib (shown in bold) are used to normalize our solutions.

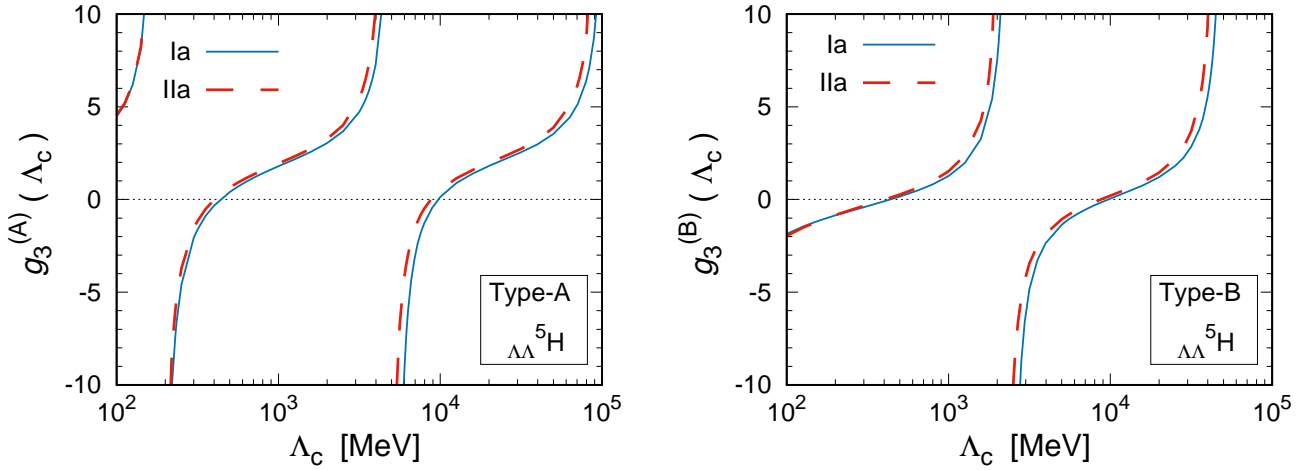


FIG. 4. The nonasymptotic RG limit cycle behaviors of the three-body couplings $g_3^{(A,B)}(\Lambda_c)$ for the $\Lambda\Lambda t$ system. Two representative choices for the S -wave double- Λ scattering lengths are considered, namely, $a_{\Lambda\Lambda} = -0.91 \text{ fm}$ (Ia) and -1.37 fm (IIa), based on the Nijmegen hard-core potential models, mND_S and ND_S, respectively [56], and compatible with the range of values constrained by the recent phenomenological analyses [36–38] of RHIC data [7]. The corresponding three-body binding or double- Λ -separation energies $B_{\Lambda\Lambda}$ (cf. Table II) used as input to our integral equations, are the predictions of the *ab initio* potential model analysis of Ref. [22]. The corresponding results for the $\Lambda\Lambda h$ system being almost identical are not displayed for brevity.

system. The characteristic quasiperiodic cyclic singularities reminiscent of the asymptotic limit cycle associated with the successive formation of three-body bound states is clearly evident in the nonasymptotic domain. Our finding in the three-body sector reveals good isospin symmetry between the two double- Λ -hypernuclear mirror partners with very little discernible difference in the RG behavior of each partner. Consequently, for brevity, we do not display the result for the $\Lambda\Lambda h$ system. As already pointed out, ideally the scale dependence of the type-A and type-B three-body couplings should be identical. However, owing to the small qualitative differences in rearrangements between the two types of elastic re-

action channels where we only choose to introduce the counterterms (cf. Figs. 2 and 3), the type-B limit cycle plots are nominally shifted leftwards and downwards with respect to the type-A limit cycle plots. In particular, due to considerable sensitivity to the small cutoff region, $\Lambda_c \lesssim 200 \text{ MeV}$, the $N = 0$ branch which is altogether washed out in the type-B plot, is still manifest in the type-A plot (top left corner). However, this branch is not associated with the formation of an Efimov state. The ground ($n = N - 1 = 0$) state on the other hand is associated with the $N = 1$ branch. Nevertheless, the regulator values, $\Lambda_c = (\Lambda_c)_N$, at which these couplings successively vanish remain unaltered in the two types of

limit cycle plots. In each case the nonasymptotic RG limit cycle parameter s_0 can be calculated via the relation

$$s_0 = \frac{\pi}{\ln \left[\frac{(\Lambda_c)_{N+1}}{(\Lambda_c)_N} \right]}; \quad N = 1, 2, \dots \quad (30)$$

where $(\Lambda_c)_N$ is the momentum cutoff corresponding to the N th zero of $g_3^{(A,B)}$. Using, say, the $N = 1, 2$ values of Λ_c we obtain $s_0 = \pi / \ln[(\Lambda_c)_2 / (\Lambda_c)_1] \approx 1.03$, which is nearly the same as the asymptotic values of s_0^∞ given in Eq. (27), irrespective of the chosen type of elastic channel. It is also notable that our s_0 or s_0^∞ values agree well with typical values anticipated from the universal calibration curve for a mass imbalanced three-body system [50], namely, the plot of $\exp(\pi/s_0)$ versus the mass ratio m_1/m_3 , with $m_1 = m_2 \equiv M_\Lambda$ and $m_3 \equiv M_T \neq m_{1,2}$.

Next we report on our regulator (Λ_c) dependence of $B_{\Lambda\Lambda}$ (cf. Fig. 5) obtained by numerically solving the homogeneous parts of the two sets of integral equations [cf. Eqs. (11) and (12)], excluding the three-body contact interaction, i.e., $g_3^{(A,B)} = 0$. Here we again consider the two representative S -wave double- Λ scattering lengths, namely, $a_{\Lambda\Lambda} = -0.91$ fm and -1.37 fm [56–58], compatible with the range, -1.92 fm $\lesssim a_{\Lambda\Lambda} \lesssim -0.5$ fm [36–38], constrained by RHIC data [7]. It may be noted that both choices (type-A and type-B) for the elastic channels yield identical cutoff dependence. Furthermore, both the double- Λ -hypernuclear mirror partners yield nearly identical results, apart from the expected “mismatch” in threshold region (see inset plot of Fig. 5). Thus, it is interesting that despite the significant spin dependent *charge symmetry breaking* reflected in the two-body binding energies, e.g., $\delta\mathcal{B}_\Lambda[0^+] \gtrsim 200$ keV, the corresponding difference of the spin-averaged binding energies, $\delta\mathcal{B}_\Lambda^{avg} \sim 5$ keV, is surprisingly small. This is easily seen using Eq. (29) with $\mathcal{B}_\Lambda^{avg}[\Lambda^4\text{H}] = 1.3395$ MeV and $\mathcal{B}_\Lambda^{avg}[\Lambda^4\text{He}] = 1.3355$ MeV, based on the recent spectroscopic measurements [8–11] [cf. Table. III and also Fig. 1]. Such a “spin averaging” effect apparently gets implicitly reflected in the unrenormalized (regulator dependent) eigenenergies, $E(\Lambda_c) \equiv -B_{\Lambda\Lambda}$, obtained via our integral equations with $g_3^{(A,B)}(\Lambda_c) = 0$. The resulting difference of the double- Λ -separation energy ($B_{\Lambda\Lambda}$) between the $(\Lambda_\Lambda^5\text{H}, \Lambda_\Lambda^5\text{He})$ mirror partners is evidently large, $\delta B_{\Lambda\Lambda}(\Lambda_{\text{crit}}^{(n=0)}) \gtrsim 200$ keV, around the particle-dimer thresholds, $\Lambda_c = \Lambda_{\text{crit}}^{(n=0)}$ (i.e., the ground ($n = 0$) state *critical cutoff* scales for the mirror partners²). However, this difference rapidly vanishes asymptotically

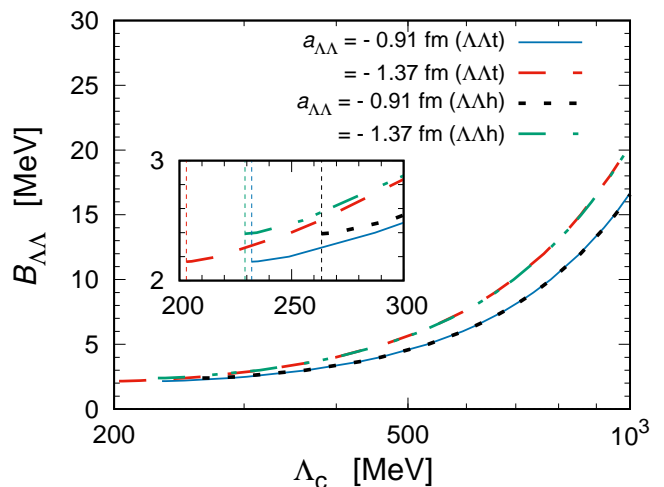


FIG. 5. The cutoff regulator (Λ_c) dependence of the three-body binding or the double- Λ -separation energy $B_{\Lambda\Lambda}$ (with respect to the three-particle threshold) of $\Lambda\Lambda T$ mirror systems with the three-body couplings $g_3^{(A,B)}$ excluded. The plots correspond to the results for both choices of the elastic channels. Two representative choices for the double- Λ scattering lengths are considered, namely, $a_{\Lambda\Lambda} = -0.91$ fm and -1.37 fm, based on the old Nijmegen hard-core potential models, mND $_S$ and ND $_S$, respectively [56], and consistent with the recent theoretical constraints [36–38] based on RHIC data [7]. The vertical lines in the inset plot denote the critical cutoffs, $\Lambda_c = \Lambda_{\text{crit}}^{(n=0)}$, defined with respect to the deeper particle-dimer thresholds, namely, the $\Lambda + u_0$ thresholds. Apart from the threshold regions, the results of both mirror partners are almost identical.

($\Lambda_c \rightarrow \infty$), ultimately leading to good charge and isospin symmetry. This feature will also be apparent in our $B_{\Lambda\Lambda} - a_{\Lambda\Lambda}$ correlation results presented later in Table. IV. Notably, due to the absence of the three-body contact interactions to renormalize the integral equations, $B_{\Lambda\Lambda}$ is quite sensitive to the cutoff variations, which increase with increasing cutoff above the respective $\Lambda + u_0$ breakup thresholds. Moreover, it is apparent that the eigenenergies are also sensitive to the input double- Λ scattering lengths, with $B_{\Lambda\Lambda}$ increasing with increasing $|a_{\Lambda\Lambda}|$.

We emphasize that, although in our EFT framework the $u_{0,1} \equiv (\Lambda T)_{s,t}$ two-body subsystems introduce two relevant energy scales $\mathcal{E}_{2(s,t)}^{thr}$, it is the larger of the two particle-dimer thresholds, namely, the $\Lambda + u_0$ (singlet-dimer) threshold that is effectively associated with the formation of Efimov states. In fact, irrespective of the chosen (type-A,B) elastic channels, our numerical evaluations of the integral equation only yield trimer states which are deeper than the $\Lambda + u_0$ thresholds, viz. $B_{\Lambda\Lambda} > \mathcal{B}_\Lambda[0^+]$ provided $\Lambda_c > \Lambda_{\text{crit}}^{(n=0)}$. No numerically stable eigensolutions are obtained in the energy domain, $\mathcal{E}_{2(s)}^{thr} < E < \mathcal{E}_{2(t)}^{thr}$, lying in between the two thresholds. Thus, we should re-emphasize the correspondence of the $\Lambda\Lambda T \rightarrow \Lambda + u_0$ breakup threshold energies $\mathcal{E}_{2(s)}^{thr}$ of the respective double- Λ -hypernuclear mirror partners

² In our case in general, $\Lambda_c = \Lambda_{\text{crit}}^{(n)}$ denotes the n th critical cutoff, defined as the cutoff scale at which the n th Efimov bound state emerges just above the *deeper* particle-dimer ($\Lambda + u_0$) breakup threshold $E = \mathcal{E}_{2(s)}^{thr}$.

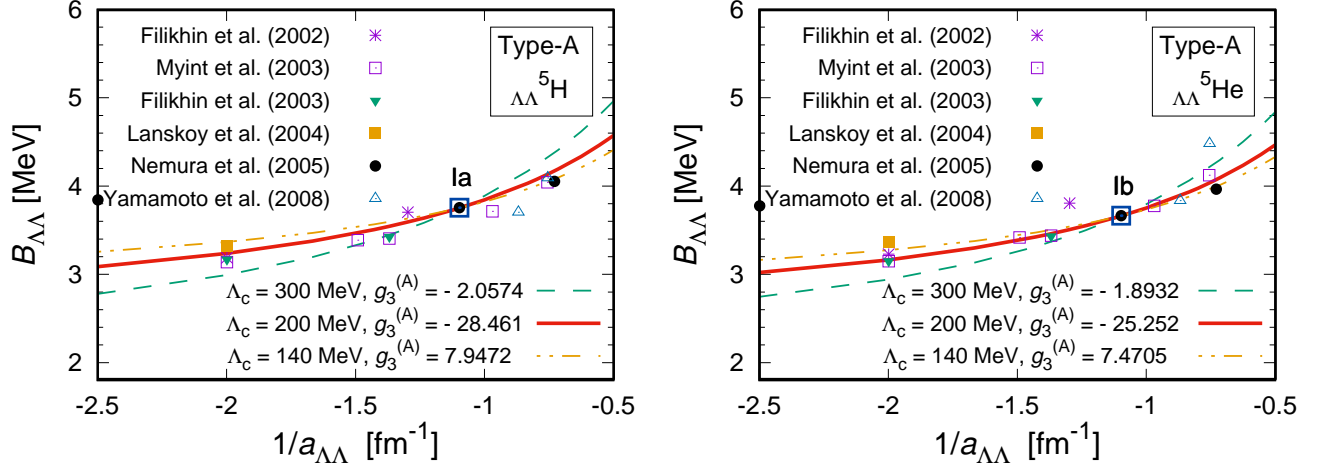


FIG. 6. The double- Λ -separation energies $B_{\Lambda\Lambda}$ of ${}^5_{\Lambda\Lambda}\text{H}$ (left panel) and ${}^5_{\Lambda\Lambda}\text{He}$ (right panel) as a function of the inverse of the S -wave double- Λ scattering length $a_{\Lambda\Lambda}^{-1}$ using different values of the three-body coupling $g_3^{(A)}$ at appropriate cutoff scales Λ_c . These results correspond to the type-A choice of the elastic channel obtained using integral equations (11). The displayed data points correspond to our reevaluations [via Eq. (28)] of the past potential model-based predictions of Refs. [16, 17, 19, 20, 22] using the current experimental input for the Λ -separation energies $\mathcal{B}_{\Lambda}[0^+, 1^+]$ of $({}^4_{\Lambda}\text{H}, {}^4_{\Lambda}\text{He})$ [8–11]. In particular, the two data points, namely, “Ia”: ($B_{\Lambda\Lambda} = 3.750$ MeV, $a_{\Lambda\Lambda} = -0.91$ fm) for ${}^5_{\Lambda\Lambda}\text{H}$ and “Ib”: ($B_{\Lambda\Lambda} = 3.660$ MeV, $a_{\Lambda\Lambda} = -0.91$ fm) for ${}^5_{\Lambda\Lambda}\text{He}$ (large open squares), taken from Ref. [22] best serve to normalize our solutions to the integral equations.

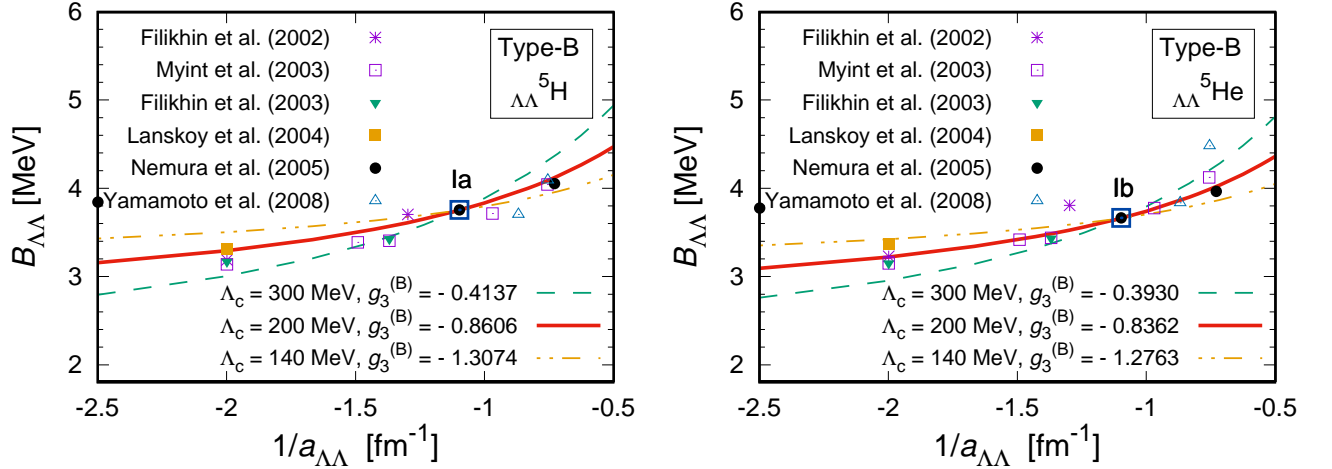


FIG. 7. The double- Λ -separation energies $B_{\Lambda\Lambda}$ of ${}^5_{\Lambda\Lambda}\text{H}$ (left panel) and ${}^5_{\Lambda\Lambda}\text{He}$ (right panel) as a function of the inverse of the S -wave double- Λ scattering length $a_{\Lambda\Lambda}^{-1}$ using different values of the three-body coupling $g_3^{(B)}$ at appropriate cutoff scales Λ_c . These results correspond to the type-B choice of the elastic channel obtained using integral equations (12). The displayed data points correspond to our reevaluations [via Eq. (28)] of the past potential model-based predictions of Refs. [16, 17, 19, 20, 22] using the current experimental input for the Λ -separation energies $\mathcal{B}_{\Lambda}[0^+, 1^+]$ of $({}^4_{\Lambda}\text{H}, {}^4_{\Lambda}\text{He})$ [8–11]. In particular, the two data points, namely, “Ia”: ($B_{\Lambda\Lambda} = 3.750$ MeV, $a_{\Lambda\Lambda} = -0.91$ fm) for ${}^5_{\Lambda\Lambda}\text{H}$ and “Ib”: ($B_{\Lambda\Lambda} = 3.660$ MeV, $a_{\Lambda\Lambda} = -0.91$ fm) for ${}^5_{\Lambda\Lambda}\text{He}$ (large open squares), taken from Ref. [22] best serve to normalize our solutions to the integral equations.

Figures 8 and 9 display the cutoff scale dependence of the Λ - $(\Lambda t)_{s,t}$ scattering lengths for the ${}^4_{\Lambda}\text{H}[0^+, 1^+]$ - Λ scattering processes for the two input double- Λ scattering lengths, namely, $a_{\Lambda\Lambda} = -0.91$ fm and -1.37 fm [56]. In this case the results for the $\Lambda\Lambda T$ mirror partners are imperceptibly close to each other, so that we graphically display the results for only one of them, say, the

$\Lambda\Lambda t$ system, although a consolidated summary of our numerical predictions for both mirror partners are tabulated in Table. IV. It is, however, worth mentioning that in contrast with our universal LO EFT prediction with very little observable difference between the $\Lambda\Lambda T$ mirrors, somewhat large isospin-breaking corrections have been reported for these systems in the context of exist-

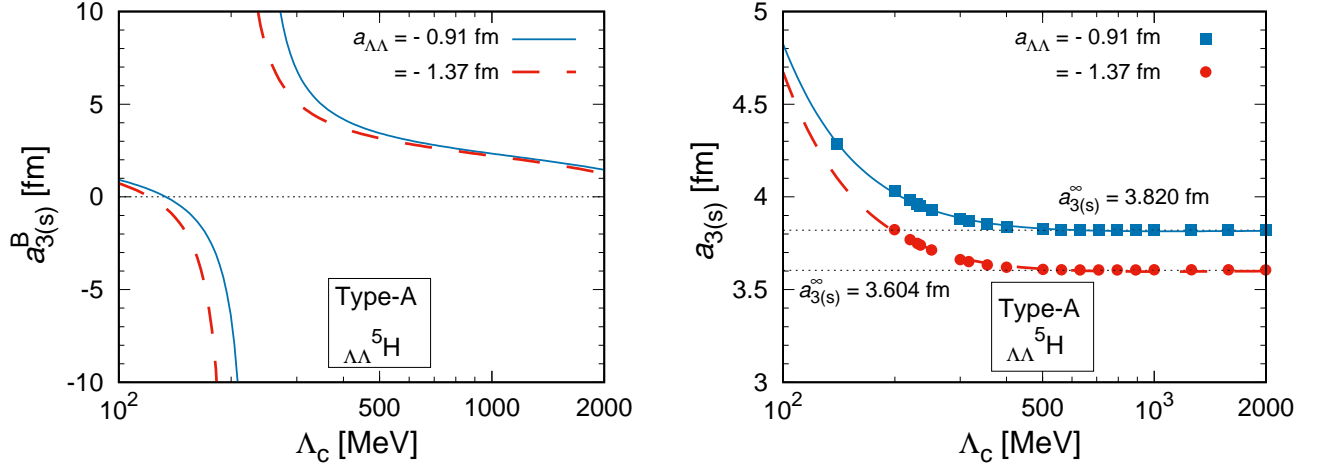


FIG. 8. The EFT predicted regulator (Λ_c) dependence of the $J = 1/2$ S -wave $\Lambda - (\Lambda t)_s$ scattering length $a_{3(s)}$ for the ${}^4_\Lambda\text{H}[0^+]$ - Λ scattering without (left panel) and with (right panel) the three-body coupling $g_3^{(A)}$. Two representative values of the Nijmegen hard-core potential model extracted double- Λ scattering lengths are used, namely, $a_{\Lambda\Lambda} = -0.91, -1.37$ fm [56], which are consistent with recent RHIC data analyses [36–38]. The input double- Λ -separation energies $B_{\Lambda\Lambda}$ needed to fix $g_3^{(A)}(\Lambda_c)$ for renormalization are obtained by using our EFT calibration curves (solid red line in Fig. 6; see also Table. IV). The unrenormalized (bare) scattering length is denoted $a_{3(s)}^B$. The smooth curves in the right panel represent fits to the data points based on the power series ansatz, Eq. (32). The corresponding results for $\Lambda\Lambda h$ or ${}^4_\Lambda\text{He}[0^+]$ - Λ scattering being very similar, are not displayed.

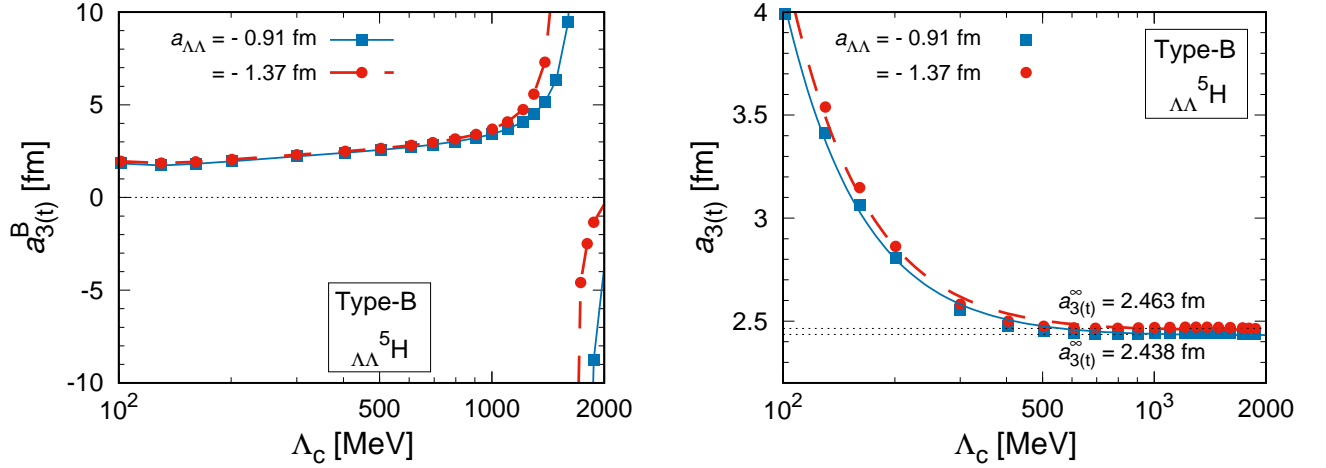


FIG. 9. The EFT predicted regulator (Λ_c) dependence of the $J = 1/2$ S -wave $\Lambda - (\Lambda t)_t$ scattering length $a_{3(t)}$ for the ${}^4_\Lambda\text{H}[1^+]$ - Λ scattering without (left panel) and with (right panel) the three-body coupling $g_3^{(B)}$. Two representative values of the Nijmegen hard-core potential model extracted double- Λ scattering lengths are used, namely, $a_{\Lambda\Lambda} = -0.91, -1.37$ fm [56], which are consistent with recent RHIC data analyses [36–38]. The input double- Λ -separation energies $B_{\Lambda\Lambda}$ needed to fix $g_3^{(B)}(\Lambda_c)$ for renormalization are obtained by using our EFT calibration curves (solid red line in Fig. 7; see also Table. IV). The unrenormalized (bare) scattering length is denoted $a_{3(t)}^B$. The smooth curves in the right panel represent fits to the data points based on the power series ansatz, Eq. (32). The corresponding results for $\Lambda\Lambda h$ or ${}^4_\Lambda\text{He}[1^+]$ - Λ scattering being very similar, are not displayed.

ing potential-model analyses. This leads to significant differences in the model predictions of the two- and three-body binding energies [20, 73]. Such precision effects are not captured without a subleading-order EFT calculation, which is beyond the present scope.

In contrast with little or no quantitative difference in results corresponding to each choice (type-A, -B) of the bound-state solutions, significant qualitative differences arise in the respective scattering domains. In the left panel plots of Figs. 8 and 9, which exclude the three-body

contact interactions, the unregulated (bare) scattering amplitudes $a_{3(s,t)}^B$ depend sensitively on the cutoff scale and diverge for specific values of Λ_c associated with the successive emergence of three-body bound states. Moreover for $\Lambda_c \lesssim 200$ MeV, the very first pole-like feature seen in the unrenormalized type-A amplitude in Fig. 8, is missing from the unrenormalized type-B amplitude displayed in Fig. 9. This feature is concomitant with the associated limit cycle behavior of the three-body systems (cf. Fig.4) where the $N = 0$ branch is found to be altogether missing in the type-B plots. Nevertheless, such unphysical singularities in the scattering amplitude are renormalized by the introduction of the scale dependent couplings $g_3^{(A,B)}(\Lambda_c)$, as revealed in the right panel plots which are free of singularities. We find that the renormalized scattering lengths $a_{3(s,t)}$ smoothly decreases with increasing Λ_c converging asymptotically for $\Lambda_c \gtrsim 500$ MeV. These asymptotic values $a_{3(s,t)}(\Lambda_c \rightarrow \infty)$ precisely yield our EFT predictions of the three-body scattering lengths corresponding to type-A,B choices of the elastic channels. To obtain the asymptotic values $a_{3(s,t)}^\infty$, we use the power series fitting ansatz for small \bar{Q}/Λ_c , namely,

$$a_{3(s,t)}(\Lambda_c) = a_{3(s,t)}^\infty \left[1 + \alpha_{s,t} \left(\frac{\bar{Q}}{\Lambda_c} \right) + \beta_{s,t} \left(\frac{\bar{Q}}{\Lambda_c} \right)^2 + \dots \right] \quad (32)$$

applied to our generated data points, as shown in the figures, obtained as solutions to the renormalized K -matrix equations (16) and (17). As estimated earlier, $\bar{Q} \sim 50$ MeV can be conveniently taken as the generic momentum scale of the underlying dynamics, with $\alpha_{s,t}$, $\beta_{s,t}$ and $a_{3(s,t)}^\infty$ being the fitting parameters. Thus, the corresponding fitting curves, as displayed Figs. 8 and 9 (right panel plots), yield the respective three-body scattering lengths by extrapolating to $\Lambda_c \rightarrow \infty$. We note that a similar *ansatz* was recently used in the SVM \mathcal{N} EFT calculation of Ref. [26] to estimate the Λ -separation energies \mathcal{B}_Λ of the $(\Lambda\Lambda^5\text{H}, \Lambda\Lambda^5\text{He})$ mirror partners.

Table. IV summarizes our numerical estimates of the S -wave renormalized type-A, -B three-body scattering lengths $a_{3(s,t)} \equiv a_{3(s,t)}(\Lambda_c \rightarrow \infty)$, as well as the *spin-averaged* values $a_{\Lambda\Lambda T}$ for different $a_{\Lambda\Lambda}$ inputs within the current theoretically feasible range, $-1.92 \text{ fm} \lesssim a_{\Lambda\Lambda} \lesssim -0.5 \text{ fm}$, based on RHIC data analyses [36–38].⁴ The chosen $a_{\Lambda\Lambda}$ values range from those extracted from the old Nijmegen potential models (e.g., NHC-F, NSC97e, ND, ND_S, mND_S) [56–58], including more recent ones based on dispersion techniques [27] and RHIC thermal correlation model analysis [36–38], and up to the most recent ones based on lattice simulations by the HAL QCD

Collaboration [35]. In particular, a representative value of $a_{\Lambda\Lambda} = -0.8 \text{ fm}$ was suggested in the recent SVM \mathcal{N} EFT calculation [26], using which \mathcal{B}_Λ of $\Lambda\Lambda^5\text{H}$ was predicted to be about 1.14 MeV. This value can be compared with our estimation displayed in Table. V, which in our $\Lambda\Lambda t$ cluster scenario may be naively obtained as

$$\begin{aligned} \mathcal{B}_\Lambda(\Lambda\Lambda^5\text{H}) &= \Delta B_{\Lambda\Lambda}(\Lambda\Lambda^5\text{H}) + \mathcal{B}_\Lambda^{avg}(\Lambda^4\text{H}) \\ &= B_{\Lambda\Lambda}(\text{Avg}) - \mathcal{B}_\Lambda^{avg}(\Lambda^4\text{H}), \end{aligned} \quad (33)$$

where

$$B_{\Lambda\Lambda}(\text{Avg}) = \frac{1}{2} [B_{\Lambda\Lambda}(\text{type-A}) + B_{\Lambda\Lambda}(\text{type-B})] \quad (34)$$

is the ordinary mean of the type-A and type-B double- Λ -separation energies of $\Lambda\Lambda^5\text{H}$ obtained from Table. IV. Likewise, we also obtain the estimate for $\mathcal{B}_\Lambda(\Lambda\Lambda^5\text{He})$, as displayed in Table. V. Consequently, the difference of the two Λ -separation energies, namely, $\mathcal{B}_\Lambda(\Lambda\Lambda^5\text{He}) - \mathcal{B}_\Lambda(\Lambda\Lambda^5\text{H}) = 9 \text{ keV}$, yields a naive estimate of the charge-symmetry-breaking effects inherent to these double- Λ -hypernuclei. This is indeed small in comparison with that in the two-body sector where $\delta\mathcal{B}_\Lambda[0^+] \sim 200 \text{ MeV}$ and $\delta\mathcal{B}_\Lambda[1^+] \sim 100 \text{ MeV}$. However, the charge asymmetry noted here does not directly reflect anything regarding the underlying low-energy EFT dynamics with no isospin breaking terms included in the effective Lagrangian at LO, but rather a consequence of using physical masses and phenomenologically fixed inputs. Nevertheless, given the broad range of acceptable input values of the S -wave double- Λ scattering lengths, namely, with $\delta a_{\Lambda\Lambda} \approx 1.42 \text{ fm}$, the corresponding variations in the spin-averaged three-body scattering lengths turn out to be quite nominal, i.e., $\delta a_{\Lambda\Lambda T} \lesssim 0.4 \text{ fm}$. But, it may be noticed that in contrast particularly the type-A scattering lengths $a_{3(s)}$ exhibit significant variations depending on the $(a_{\Lambda\Lambda}, B_{\Lambda\Lambda})$ inputs. In fact the behavior, of $a_{3(s)}$ and $a_{3(t)}$ are turn out to be quite the opposite, with the former increasing and the latter decreasing with both $|a_{\Lambda\Lambda}|$ and $B_{\Lambda\Lambda}$ decreasing.

The above discussed features are depicted clearly in the Phillips-line plots [59] shown in upper the panels of Fig. 10, for each choice (type-A, -B) of the elastic channel. Interestingly, the variation of the spin-averaged scattering length $a_{\Lambda\Lambda T}$, in what may be termed as the ‘‘physical’’ Phillips plot (lower panel) turns out to be significantly moderate. Evidently, the type-A Phillips plots are in accordance with the expected behavior of the three-body binding energies varying inversely as the three-body scattering lengths, accounting for their characteristic negative slopes. In contrast, the observed positive slope of the type-B Phillips plot may seem rather counterintuitive. It is noteworthy that these contrasting type-A, -B results are neither dependent on the nature of the three-body contact interactions used nor any artifact of the renormalization methods adopted in each case [cf. discussion below Eq. (15)]. This is easily understood by comparing the plots for the unrenormalized type-A, -B scattering lengths, which exhibit the same contrasting features.

⁴ In contrast, the same RHIC data previously analyzed by the STAR Collaboration [7] suggested a positive value of the scattering length. It is notable, however, that our analysis in this work is *only* justified on the basis of a virtual bound $\Lambda\Lambda$ state. Hence, we restrict our analysis to negative $a_{\Lambda\Lambda}$ values only.

Hypernucleus ($J = \frac{1}{2}$)	Scattering length $a_{\Lambda\Lambda}$ (fm)	Type-A $B_{\Lambda\Lambda}$ (MeV)	Type-A $a_{3(s)}(\Lambda_c \rightarrow \infty)$ (fm)	Type-B $B_{\Lambda\Lambda}$ (MeV)	Type-B $a_{3(t)}(\Lambda_c \rightarrow \infty)$ (fm)	($2J + 1$) average $a_{\Lambda\Lambda T}$ (fm)
${}^5_{\Lambda\Lambda}\text{H}$	-0.50 (NSC97e) [57, 58]	3.236	4.258	3.292	2.388	2.968
	-0.60 (DR) [27]	3.377	4.109	3.418	2.404	2.925
	-0.73 (NHC-F) [56]	3.544	3.964	3.567	2.420	2.885
	-0.77 (ND) [57, 58]	3.592	3.927	3.610	2.425	2.875
	-0.80 (SVM) [26]	3.627	3.902	3.641	2.428	2.868
	-0.81 (HAL QCD) [35]	3.639	3.894	3.651	2.429	2.866
	-0.91 (mND _S) [56]	3.750 [22]	3.821	3.750 [22]	2.438	2.847
	-1.20 (DR) [27]	4.030	3.668	3.997	2.456	2.809
	-1.25 (RHIC) [36–38]	4.073	3.648	4.034	2.459	2.804
	-1.32 (NHC-F) [56]	4.131	3.622	4.085	2.462	2.797
	-1.37 (ND _S) [56]	4.170	3.605	4.119	2.463	2.793
	-1.80 (DR) [27]	4.461	3.493	4.374	2.473	2.764
-1.92 (RHIC) [36–38]	4.530	3.470	4.434	2.474	2.757	
${}^5_{\Lambda\Lambda}\text{He}$	-0.50 (NSC97e) [57, 58]	3.163	4.714	3.221	1.831	2.841
	-0.60 (DR) [27]	3.298	4.461	3.341	1.837	2.740
	-0.73 (NHC-F) [56]	3.460	4.229	3.484	1.843	2.649
	-0.77 (ND) [57, 58]	3.506	4.173	3.525	1.845	2.628
	-0.80 (SVM) [26]	3.541	4.134	3.555	1.846	2.613
	-0.81 (HAL QCD) [35]	3.552	4.121	3.565	1.846	2.608
	-0.91 (mND _S) [56]	3.660 [22]	4.012	3.660 [22]	1.849	2.567
	-1.20 (DR) [27]	3.934	3.793	3.899	1.853	2.485
	-1.25 (RHIC) [36–38]	3.976	3.766	3.935	1.854	2.474
	-1.32(NHC-F) [56]	4.032	3.730	3.984	1.854	2.461
	-1.37(ND _S) [56]	4.071	3.707	4.018	1.854	2.452
	-1.80 (DR) [27]	4.357	3.558	4.266	1.853	2.396
-1.92 (RHIC) [36–38]	4.425	3.528	4.324	1.852	2.384	

TABLE IV. The EFT predicted $J = 1/2$ S -wave $\Lambda\Lambda T$ scattering lengths $a_{\Lambda\Lambda T}$ [cf. Eq. (24)] of the double- Λ -hypernuclear mirror partners (${}^5_{\Lambda\Lambda}\text{H}$, ${}^5_{\Lambda\Lambda}\text{He}$), obtained for the central values of the S -wave scattering length $a_{\Lambda\Lambda}$ based on various phenomenological analyses, e.g., old Nijmegen potential models (e.g., NHC-F, NSC97e, ND, ND_S, mND_S) [56–58], dispersion relations (DR) [27], thermal correlation model of relativistic heavy-ion collisions (RHIC) [36–38], *ab initio* $^{\#}$ EFT (SVM) [26], and lattice QCD (HAL QCD) [35], consistent with the currently accepted range, $-1.92 \text{ fm} \lesssim a_{\Lambda\Lambda} \lesssim -0.5 \text{ fm}$ [36–38]. All the displayed double- Λ -separation energies $B_{\Lambda\Lambda}$, excepting the two normalization values taken from the potential model *ab initio* SVM analysis of Ref. [22] (shown in bold), are obtained using our calibration curves for the choice of the cutoff scale, $\Lambda_c = 200 \text{ MeV}$.

Hypernucleus ($J = \frac{1}{2}, I = \frac{1}{2}$)	This work, Eq. (33) \mathcal{B}_{Λ} (MeV)	Ref. [26] \mathcal{B}_{Λ} (MeV)
${}^5_{\Lambda\Lambda}\text{H}$	2.295	$1.14 \pm 0.01^{+0.44}_{-0.26}$
${}^5_{\Lambda\Lambda}\text{He}$	2.212	-

TABLE V. The Λ -separation energies, namely, $\mathcal{B}_{\Lambda}({}^5_{\Lambda\Lambda}\text{H})$ and $\mathcal{B}_{\Lambda}({}^5_{\Lambda\Lambda}\text{He})$, corresponding the representative value, $a_{\Lambda\Lambda} = -0.80 \text{ fm}$. The result for ${}^5_{\Lambda\Lambda}\text{H}$ of Ref. [26] is displayed for comparison.

In this context, we also note that in determining $a_{3(s)}$, only the dynamics near the deeper threshold, namely, the particle-dimer $\Lambda + u_0$ threshold, is relevant, whereas the dynamics of both thresholds ($\Lambda + u_{0,1}$) contribute in the determination of $a_{3(t)}$. Although an unambiguous physical reasoning behind this contrasting behavior could not be ascertained, a plausible explanation may be attributed to the underlying nature of the off-shell dynamics arising due to the complex interplay between the two thresholds.

To test this hypothesis we took the strategy of considering a hypothetical (unphysical) scenario in which the

triplet and singlet ΛT subsystems are completely decoupled from each other to avoid the simultaneous contribution of both the particle-dimer thresholds for each $\Lambda\Lambda T$ systems. In other words, this is essentially tantamount to the removal of the triplet-dimer field u_1 contributions in the type-A integral equations (11), and the singlet-dimer field u_0 contributions in the type-B integral equations (12). The resulting $\Lambda\Lambda T$ dynamics become considerably simpler reducing into a system of two coupled-channel integral equations in each case. It is found that, in these reduced systems, the type-A elastic channel does not exhibit a limit cycle behavior any longer, while the type-B elastic channels continue to exhibit limit cycles but instead following a very different value of the asymptotic parameter, namely, $s_0^{\infty} \approx 0.84$, for each mirror system. Subsequently, it may indeed be checked that the estimation of the scattering lengths $a_{3(s,t)}$ leads to the expected natures of the Phillips-lines with negative slopes. This ostensibly indicates plausible role of the simultaneous particle-dimer thresholds resulting in the atypical nature of the type-B Phillips-lines. However, a more satisfactory explanation of this feature demands a thorough

understanding of the off-shell dynamics perhaps hinting at the need of a four-body calculations which is beyond the present scope. Finally, the fact that our results converge asymptotically for momentum scales significantly larger than m_π , the canonical hard scale of $\not\text{EFT}$, there is an indication of the apparent insensitivity of the three-body dynamics to the Λ - Λ (two-body) correlations. In this regard, our findings corroborate the two previous $\not\text{EFT}$ analyses [24, 25] based on similar three-body calculations of ${}^4_{\Lambda\Lambda}\text{H}$ and ${}^6_{\Lambda\Lambda}\text{He}$ double- Λ -hypernuclei.

IV. SUMMARY AND CONCLUSIONS

In summary, this work presents an assay of the putative doubly strange ($S = -2$) mirror double- Λ -hypernuclei (${}^5_{\Lambda\Lambda}\text{H}$, ${}^5_{\Lambda\Lambda}\text{He}$) in the context of a LO pionless EFT. In this framework the systems are conjectured as shallow three-particle halo-bound clusters, viz. the iso-doublet pair ($\Lambda\Lambda t$, $\Lambda\Lambda h$) in the $J = 1/2$ channel. The numerical methodology presented here closely resembles the approaches of Refs. [24, 25, 51, 52]. By solving the Faddeev-like coupled integral equations [65–68] for each choice (type-A, -B) of the constituent $(\Lambda T)_{s,t}$ subsystem spin introduced in the elastic channel, we presented a qualitative RG based study of the cutoff dependence of the three-body contact interactions. In particular, we investigated the dynamical interplay between the different constituent two-body subsystems, namely, the virtual bound 1S_0 $\Lambda\Lambda$ cluster (with $a_{\Lambda\Lambda} < 0$), and the $(\Lambda T)_{s,t}$ bound clusters (equivalently, the two-body spin-singlet and spin-triplet bound states, i.e., ${}^4_{\Lambda}\text{H}[J = 0^+, 1^+]$ and ${}^4_{\Lambda}\text{He}[J = 0^+, 1^+]$), whose interplay could plausibly lead to the emergence of three-body shallow bound states. This is formally suggested by the appearance of RG limit cycles in the running of the three-body couplings $g_3^{(A,B)}(\Lambda_c)$. In the unitary limit this also implies that a discrete sequence of Efimov states emerges from the three-particle threshold [54], and simultaneously with our LO theory in the *scaling limit*, the ground-state energy collapses to negative infinity (Thomas effect [74]). Of course, such universal phenomena are *de facto* unrealistic and disappear for interactions with nonvanishing range (finite momentum cutoff) and finite scattering lengths. Nevertheless, for energies in proximity to the particle-dimer thresholds (sufficiently far from open channels involving transmutations into particles like Σ , Ξ , \dots) with reasonably fine-tuned Λ - T and Λ - Λ correlation strengths, it can not be precluded that any remnant universal feature leads to the formation of Efimov-like trimers.

For our numerical analysis we considered different choices of the input double- Λ scattering lengths within the currently acceptable range, $-1.92 \text{ fm} \lesssim a_{\Lambda\Lambda} \lesssim -0.5 \text{ fm}$ [36–38], along with the inputs for the $\Lambda + u_{0,1}$ particle-dimer thresholds provided by the up-to-date experimental information on the Λ -separation energies of the (${}^4_{\Lambda}\text{H}$, ${}^4_{\Lambda}\text{He}$) mirror hypernuclei [3, 8–11]. By appropriate fixing of the three-body contact interactions

using the RG limit cycles at the typical cutoff scale, $\Lambda_c \sim 200 \text{ MeV}$, a fairly good agreement of our EFT predicted $B_{\Lambda\Lambda}$ - $a_{\Lambda\Lambda}$ correlations was obtained with existing potential models [16, 17, 19, 20, 22] (provided that the $B_{\Lambda\Lambda}$ are reevaluated from their old model prediction of $B_{\Lambda\Lambda}$ using updated experimental inputs). This agreement, of course, relied on the efficacy in choosing our normalization points, taken from the *ab initio* potential model analysis of Nemura *et al.* [22]. In this case the double- Λ -separation energy $B_{\Lambda\Lambda}$ could be identified with the eigenenergy of the ground ($n = 0$) state Efimov-like trimer, with the provision that our halo/cluster $\not\text{EFT}$ analysis could be extended to include $\pi\pi$ or σ -meson exchange interactions with an adjusted breakdown scale, $\Lambda_H \gtrsim 2m_\pi$. But whether such physically realizable bound states can be *de facto* supported in our EFT framework remains contentious, depending crucially on support from experimental or lattice QCD data which are currently altogether missing. Future feasibility studies from the much awaited production experiments, like PANDA and CBM at FAIR [75–77], and JPARC-P75 [78], are likely to explicate more on the inherent character of these hypernuclei. Besides, predictions based on LO EFT analyses are by and large qualitative in nature and must be supplemented by subleading order precision analyses for robust assessments. This should naturally address issues such as the compatibility of the low-energy cluster picture at momentum scales, $Q \gtrsim \Lambda_H$, potentially probing the short-distance degrees of freedom beyond the breakup scales of the triton and helion cores.

Finally, to demonstrate the predictive power of our EFT analysis, we presented preliminary estimates of the Λ -separation energies \mathcal{B}_Λ of the two double- Λ -hypernuclear mirrors of interest and the previously undetermined S -wave three-body scattering lengths for the ${}^4_{\Lambda}\text{H}$ - Λ and ${}^4_{\Lambda}\text{He}$ - Λ scattering processes. Needless to say that, with the scarcity of pertinent empirical inputs, a theoretical error analysis based on such empirical estimates serves little purpose and, hence, was not attempted in this work. Nevertheless, the accuracy of our results evidently relies on the precise nature of the $B_{\Lambda\Lambda}$ - $a_{\Lambda\Lambda}$ correlations, with the latter being still poorly constrained currently. Subject to the inherent limitation pertaining to the ambiguity in the normalization of the solutions to the integrals equations, our EFT methodology demands a three-body empirical input which is provided by the $B_{\Lambda\Lambda}$ model predictions of Nemura *et al.* Subsequently, the correlation plots self-consistently determine the three-body scattering lengths $a_{\Lambda\Lambda T}$. In particular, the scale variation of the renormalized scattering lengths was found to asymptotically converge for $\Lambda_c \gtrsim 500 \text{ MeV}$ which is well beyond the hard scale of standard $\not\text{EFT}$. Thus, the three-body dynamics are most likely insensitive to the low-energy Λ - Λ two-body interactions, unless the hard-scale Λ_H of the effective theory could be augmented sufficiently beyond without potentially invalidating the basic halo/cluster *ansatz*. This supports the earlier claim made in Refs. [24, 25]

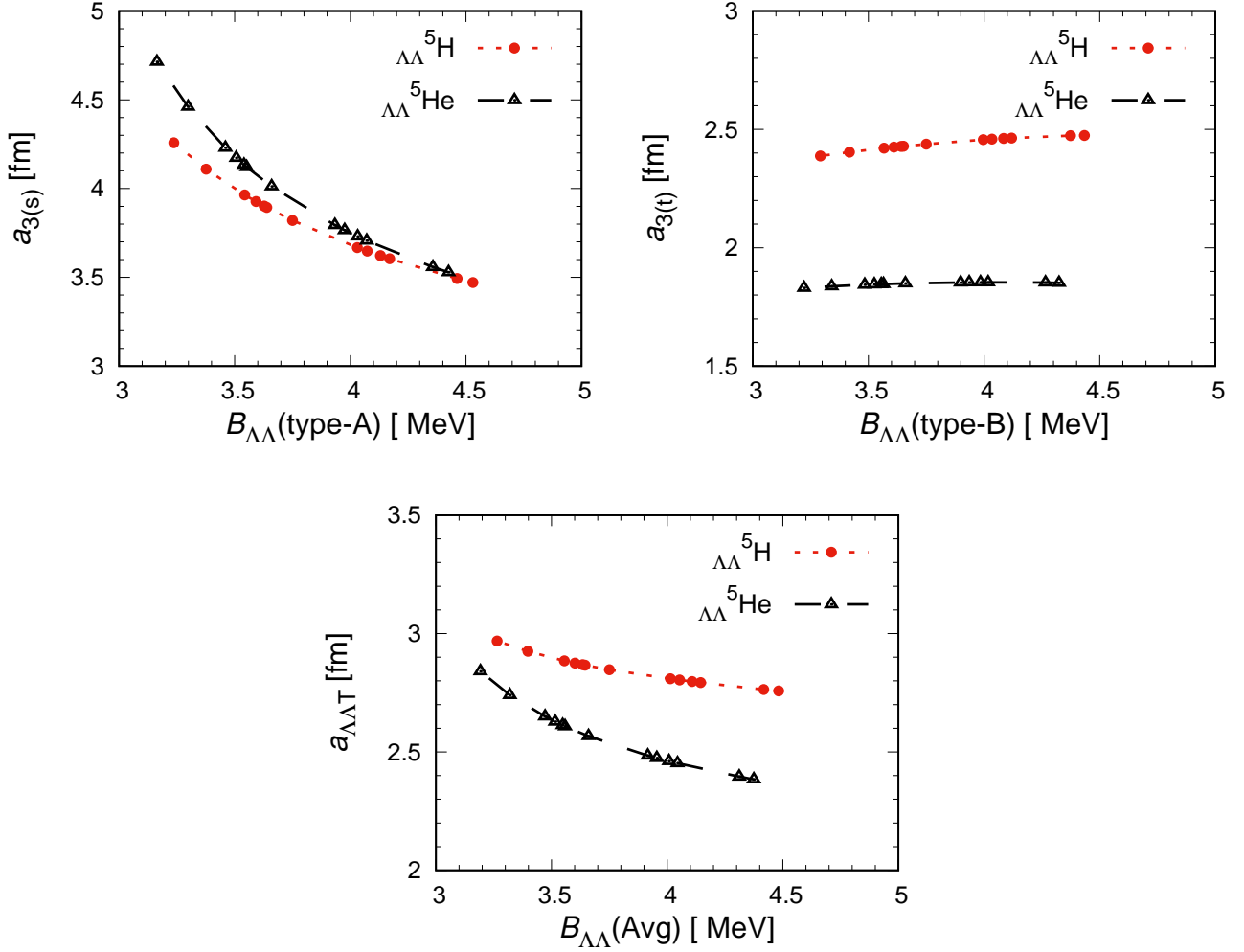


FIG. 10. Phillips-lines for the type-A elastic channel, i.e., ${}^4_{\Lambda\Lambda}\text{H}[0^+]$ - Λ and ${}^4_{\Lambda\Lambda}\text{He}[0^+]$ - Λ scatterings (upper left panel) and the type-B elastic channel, i.e., ${}^4_{\Lambda\Lambda}\text{H}[1^+]$ - Λ and ${}^4_{\Lambda\Lambda}\text{He}[1^+]$ - Λ scatterings (upper right panel) are displayed. The lower panel displays the “physical” Phillips-lines corresponding to the spin-averaged scattering lengths $a_{\Lambda\Lambda T}$ plotted as a function the mean values of the three-body binding energy, namely, $B_{\Lambda\Lambda}(\text{Avg}) = \frac{1}{2} [B_{\Lambda\Lambda}(\text{type-A}) + B_{\Lambda\Lambda}(\text{type-B})]$, obtained from Table. IV.

based on similar investigations of the other double- Λ -hypernuclear cluster systems, such as ${}^4_{\Lambda\Lambda}\text{H}$ and ${}^6_{\Lambda\Lambda}\text{He}$. Although short-distance mechanisms beyond the realm of our EFT can certainly influence the formation of such exotic bound hypernuclear clusters, this does not preclude possible role of low-energy off-shell effects that may not be accessible in a three-body framework without involving four-body calculations. Such an endeavor, however, goes beyond the scope of the simple qualitative nature of this work. To this end, we reiterate once more that our estimates of the scattering lengths $a_{\Lambda\Lambda T}$ should serve for demonstrative purposes only, given the current limitations of performing $\Lambda\Lambda T$ scattering experiments in testing their validity thereof.

ACKNOWLEDGMENTS

We are thankful to S.-I. Ando for providing many useful suggestions regarding this work. We are also thankful to A. Gal for apprising us of the pioneering work of Ref. [26] on the *ab initio* (SVM) pionless EFT analysis regarding the onset of double- Λ -hypernuclear binding.

V. APPENDIX

A. One- and Two-body non-relativistic Propagators

Here we summarize the one- and two-body nonrelativistic propagators specific to the $\Lambda\Lambda T$ three-body systems in pionless effective theory (${}^{\Lambda}\text{EFT}$). In this frame-

work, at sufficiently low-energies below the respective breakup scales, we may consider the triton (${}^3\text{H}$ or t) and the helion (${}^3\text{He}$ or h) as being fundamental particles. Thus, as the fundamental one-body components of the theory, the Λ and T propagators are given as

$$iS_{\Lambda,T}(p_0, \mathbf{p}) = \frac{i}{p_0 - \frac{\mathbf{p}^2}{2M_{\Lambda,T}} + i\eta}, \quad (35)$$

where p_0 and \mathbf{p} are the generic off-shell energy and three-momentum. In our analysis we only consider the S -waves contributions from the two-body interactions at LO. We have incorporated a power counting scheme [44, 45] for the ${}^1\text{S}_0$ Λ - T , ${}^3\text{S}_1$ Λ - T and the ${}^1\text{S}_0$ Λ - Λ interactions in the two-body sector, in which the unitarized two-body amplitudes are conveniently expressed in terms of the auxiliary fields, namely, the spin-singlet and spin-triplet ΛT -dimer fields $u_{0,1}$, and the spin-singlet $\Lambda\Lambda$ -dibaryon field u_s . The leading order renormalized dressed dimer propagators [47–49] are given by the expressions (see Fig. 11)

$$D_{0,1}(p_0, \mathbf{p}) = \frac{1}{\gamma_{0,1} - \sqrt{-2\mu_{\Lambda T}(p_0 - \frac{\mathbf{p}^2}{2(M_T + M_\Lambda)}) - i\eta} - i\eta}, \quad (36)$$

and,

$$\mathcal{D}_s(p_0, \mathbf{p}) = \frac{1}{\frac{1}{a_{\Lambda\Lambda}} - \sqrt{-M_\Lambda(p_0 - \frac{\mathbf{p}^2}{4M_\Lambda}) - i\eta} - i\eta}, \quad (37)$$

respectively, with the LO two-body contact interactions y_0 , y_1 , and y_s fixed as in Eq. (8) in the text. In the above expressions, γ_0 and γ_1 are the binding momenta of spin-singlet and spin-triplet states of the ΛT subsystem, and $a_{\Lambda\Lambda}$ is S -wave double- Λ scattering length.

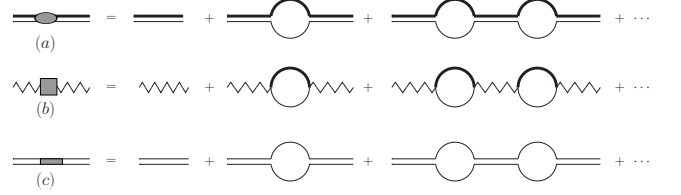


FIG. 11. Diagrams for the renormalized dressed dimer propagators: (a) $i\Delta_0$ for the spin-singlet auxiliary field u_0 , (b) $i\Delta_1$ for the spin-triplet auxiliary field u_1 , and (c) $i\Delta_s$ for the spin-singlet auxiliary field u_s . Thick (thin) lines denote the Λ -hyperon (core $T \equiv t, h$) field propagators.

-
- [1] H. Takahashi *et al.*, Phys. Rev. Lett. **87**, 212502 (2001).
[2] J. K. Ahn *et al.*, Phys. Rev. Lett. **87**, 132504 (2001).
[3] D. H. Davis, Nucl. Phys. A **754** (2005) 3c.
[4] C. J. Yoon *et al.* [E522 (KEK-PS) Collaboration], Phys. Rev. C **75**, 022201(R) (2007).
[5] J. K. Ahn *et al.* [E373 (KEK-PS) Collaboration], Phys. Rev. C **88**, no. 1, 014003 (2013).
[6] H. Tamura *et al.*, Nucl. Phys. A **914**, 99 (2013).
[7] L. Adamczyk *et al.* [STAR Collaboration], Phys. Rev. Lett. **114**, 022301 (2015).
[8] T. Yamamoto *et al.* [J-PARC E13 Collaboration], Phys. Rev. Lett. **115**, 222501 (2015).
[9] A. Esser *et al.* [A1 Collaboration], Phys. Rev. Lett. **114**, 232501 (2015).
[10] F. Schulz *et al.* [A1 Collaboration], Nucl. Phys. A **954**, 149-160 (2016).
[11] T. Koike *et al.* [J-PARC E13 Collaboration], AIP Conf. Proc. **2130**, No.1, 020011 (2019).
[12] S. Achariya *et al.* [ALICE Collaboration], Phys. Rev. C **99**, 024001 (2019).
[13] S. Achariya *et al.* [ALICE Collaboration], Phys. Lett. B **797**, 134822 (2019).
[14] R. L. Jaffe, Phys. Rev. Lett. **38**, 195 (1977).
[15] H. W. Hammer, Nucl. Phys. A **705**, 173 (2002).
[16] I. N. Filikhin and A. Gal, Nucl. Phys. A **707**, 491 (2002).
[17] I. N. Filikhin, A. Gal and V. M. Suslov, Phys. Rev. C **68**, 024002 (2003).
[18] H. Nemura, Y. Akaishi and K. S. Myint, Phys. Rev. C **67**, 051001 (2003).
[19] K. S. Myint, S. Shinmura and Y. Akaishi, Eur. Phys. J. A **16**, 21 (2003).
[20] D. E. Lansky and Y. Yamamoto, Phys. Rev. C **69**, 014303 (2004).
[21] M. Shoeb, Phys. Rev. C **69**, 054003 (2004).
[22] H. Nemura, S. Shinmura, Y. Akaishi and K. S. Myint, Phys. Rev. Lett. **94**, 202502 (2005).
[23] H. Nemura, S. Shinmura, Y. Akaishi and K. S. Myint, Nucl. Phys. A **754**, 110 (2005).
[24] S.-I. Ando, G.-S. Yang and Y. Oh, Phys. Rev. C **89**, 014318 (2014).
[25] S.-I. Ando and Y. Oh, Phys. Rev. C **90**, 037301 (2014).
[26] L. Contessi *et al.*, Phys. Lett. B **797**, 134893 (2019).
[27] A. M. Gasparyan, J. Haidenbauer and C. Hanhart, Phys. Rev. C **85**, 015204 (2012).
[28] S. R. Beane *et al.* [NPLQCD Collaboration], Phys. Rev. Lett. **106**, 162001 (2011).
[29] S. R. Beane *et al.* [NPLQCD Collaboration], Mod. Phys. Lett. A **26** 2587 (2011).
[30] S. R. Beane *et al.* [NPLQCD Collaboration], Phys. Rev. D **85**, 054511 (2011).
[31] T. Inoue *et al.* [HAL QCD Collaboration], Phys. Rev. Lett. **106**, 162002 (2011).
[32] T. Inoue *et al.* [HAL QCD Collaboration], AIP Conference Proceedings 1441, 335 (2012).
[33] P. E. Shanahan, A. W. Thomas and R. D. Young, Phys. Rev. Lett. **107**, 092004 (2011).
[34] J. Haidenbauer and Ulf.-G. Meissner, Phys. Lett. B **708**, 100 (2011).
[35] K. Sasaki *et al.* [HAL QCD Collaboration], Nucl. Phys. A **998**, 121737 (2020).
[36] K. Morita, T. Furumoto and A. Ohnishi, Phys. Rev. C **91**, 024916 (2015).

- [37] A. Ohnishi, K. Morita and T. Furumoto, JPS Conf. Proc. **17**, 031003 (2017)
- [38] A. Ohnishi, K. Morita, K. Miyahara, and T. Hyodo, Nucl. Phys. A **954**, 294 (2016).
- [39] N. Barnea *et al.*, Phys. Rev. Lett. **114**, 052501 (2015).
- [40] A. Kirscher *et al.*, Phys. Rev. C **92**, 054002 (2015).
- [41] A. Kirscher *et al.*, Phys. Rev. C **96**, 024001 (2017).
- [42] L. Contessi, N. Barnea and A. Gal, Phys. Rev. Lett. **121**, 102502 (2018).
- [43] M. Juric *et al.*, Nucl. Phys. B **52**, 1 (1973).
- [44] D. B. Kaplan, M. J. Savage and M. B. Wise, Phys. Lett. B **424**, 390 (1998).
- [45] D. B. Kaplan, M. J. Savage and M. B. Wise, Nucl. Phys. B **534**, 329 (1998).
- [46] U. van Kolck, Nucl. Phys. A **645**, 273-302 (1999).
- [47] P. F. Bedaque, H. W. Hammer and U. van Kolck, Phys. Rev. Lett. **82**, 463 (1999).
- [48] P. F. Bedaque, H. W. Hammer and U. van Kolck, Nucl. Phys. A **646**, 444 (1999).
- [49] P. F. Bedaque, H. W. Hammer and U. van Kolck, Nucl. Phys. A **676**, 357 (2000).
- [50] E. Braaten and H.-W. Hammer, Phys. Rept. **428**, 259 (2006).
- [51] S. I. Ando, U. Raha and Y. Oh, Phys. Rev. C **92**, no. 2, 024325 (2015).
- [52] U. Raha, Y. Kamiya, S. I. Ando, and T. Hyodo, Phys. Rev. C **98**, no. 3, 034002 (2018).
- [53] D. Gazda and A. Gal, Nucl. Phys. A **954**, 161-175 (2016).
- [54] V. Efimov, Phys. Lett. B **33**, 563 (1970).
- [55] F. Hildenbrand and H.-W. Hammer, Phys. Rev. C **100**, 034002 (2019).
- [56] M. .M. Nagels, T. A. Rijken, and J. J. de Swart, Phys. Rev. D **15**, 2547 (1977); **20**, 1633 (1979).
- [57] T. A. Rijken, V. G. J. Stoks, and Y. Yamamoto, Phys. Rev. C **59**, 21 (1999).
- [58] V. G. J. Stoks and Th. A. Rijken, Phys. Rev. C **59**, 3009 (1999).
- [59] A. C. Phillips, Nucl. Phys. A **107**, 209 (1968).
- [60] S. R. Beane and M. J. Savage, Nucl. Phys. A **694**, 511 (2001).
- [61] S.-I. Ando and C. H. Hyun, Phys. Rev. C **72**, 014008 (2005).
- [62] S. I. Ando and M. C. Birse, J. Phys. G **37**, 105108 (2010).
- [63] H. W. Griesshammer, Nucl. Phys. A **744**, 192 (2004).
- [64] K. G. Wilson, Phys. Rev. D **3**, 1818 (1971).
- [65] G. V. Skornyakov and K. A. Ter-Martirosyan, Sov. Phys. JETP **4**, 648 (1957) [Zh. Eksp. Teor. Fiz. 31, 775 (1956)].
- [66] G. V. Skornyakov and K. A. Ter-Martirosyan, JETP **31**, 775 (1956).
- [67] G. S. Danilov, Zh. Eksp. Teor. **40**, 498 (1961) [Sov. Phys. JETP **13**, 349 (1961)].
- [68] G. S. Danilov and V. I. Lebedev, Sov. Phys. JETP **17**, 1015 (1963).
- [69] P. J. Mohr, D. B. Newell and B. N. Taylor, Rev. Mod. Phys. **88**, no.3, 035009 (2016).
- [70] K. L. Kowalski, Phys. Rev. Lett. **15**, 798 (1965).
- [71] H. P. Noyes, Phys. Rev. Lett. **15**, 538 (1965).
- [72] W. Glöckle, *The Quantum Mechanical Few-Body Problem*, (Text and Monographs in Physics, Springer-Verlag, Heidelberg, 1983).
- [73] A. Gal, Phys. Lett. B **744**, 352 (2015).
- [74] L. H. Thomas, Phys. Rev. **47**, 903 (1935).
- [75] J. Pochodzalla *et al.* [PANDA Collaboration], EPJ Web of Conferences **3**, 07008 (2010).
- [76] G. Boca *et al.* [PANDA Collaboration], EPJ Web of Conferences **95**, 01001 (2015).
- [77] I. Vassiliev *et al.* [CBM Collaboration], JPS Conf. Proc. **17**, 092001 (2017).
- [78] H. Fujioka *et al.* [JPARC Collaboration], AIP Conference Proceedings **2130**, 040002 (2019).